Mice Mucosal Leishmaniasis model shown high parasite load, increased cytotoxicity and impaired IL-10^{+} cells response

Alisson Amaral da Rocha[1,2]; Júlio Souza dos Santos[1,2]; Igor Bittencourt dos Santos[1,2]; Douglas B. de Almeida[1,2]; Naiara Carla dos Santos Manhães[1,2]; Hozany Praxedes dos Santos[1,2]; João Victor Paiva Romano[1,2]; Elias Barbosa da Silva Junior[3]; Antônio José da Silva Gonçalves[4]; Marcia Pereira de Oliveira Duarte[4]; Luciana Polaco Covre[5]; Daniel Claudio de Oliveira Gomes[5]; Alda Maria da Cruz[4]; Alessandra Marcia da Fonseca Martins[1,2]; Herbert Leonel de Matos Guedes[1,2].

[1] Instituto de Microbiologia Paulo de Góes – Universidade Federal do Rio de Janeiro. City: Rio de Janeiro. State: Rio de Janeiro. Country: Brazil; Postal Code: 21941-902

[2] Laboratório de Imunologia Clínica, Instituto Oswaldo Cruz, Fundação Oswaldo Cruz, Rio de Janeiro, RJ, Brazil; Postal Code: 21040-360

[3] Instituto de Biofísica Carlos Chagas Filho – Universidade Federal do Rio de Janeiro, City: Rio de Janeiro. State: Rio de Janeiro. Country: Brazil[1]; Postal Code: 21941-902

[4] Laboratório Interdisciplinar de Pesquisas Médicas, Instituto Oswaldo Cruz, Fundação Oswaldo Cruz, Rio de Janeiro, RJ, Brazil. 21040-900

[5] Núcleo de Doenças Infecciosas – Universidade Federal do Espírito Santo. City: Vitória. State: Espírito Santo. Country: Brazil; Postal Code: 29047-100

Authors Publication Name:

Da-Rocha. A.A.[1,2]; Dos-Santos, J.S.[1,2]; Bittencourt, I.S.[1,2]; De-Almeida, D.B.[1,2]; Manhães, N.C.S.[1,2]; Praxedes, H.[1,2]; Romano J.V.P.[1,2]; Silva-Junior, E.B.[3]; Silva-Gonçalves, A. J.[4]; Oliveira[4], M.P.; Covre L.P.[5]; Oliveira-Gomes, D.C.[5]; Da-Cruz, A. M.[4]; da Fonseca-Martins, A.M.[1,2]; de Matos Guedes, H. L.[1,2].

Footnote Page

Corresponding Author:

Dr. Herbert Leonel de Matos Guedes

E-mail: herbert@micro.ufrj.br; herbert@ioc.fiocruz.br

Universidade Federal do Rio de Janeiro, Instituto de Microbiologia Paulo de Góes, Grupo de Imunologia e Vacinologia, Laboratório de Imunobiotecnologia, Av. Carlos Chagas Filho, 373, CCS, Room I2-043, Rio de Janeiro, 21941-902. RJ, Brazil. Phone: +55 21 3239-6509

Laboratório de Imunologia Clínica, Instituto Oswaldo Cruz, Fundação Oswaldo Cruz, Rio de Janeiro, RJ, Brazil; Postal Code: 21040-360

Conflict of Interest:

Da-Rocha. A.A. (No Conflict); Dos-Santos, J.S. (No Conflict); Bittencourt, I.S. (No Conflict); De-Almeida, D.B. (No Conflict); Manhães, N.C.S. (No Conflict); Praxedes, H. (No Conflict); Romano J.V.P. (No Conflict); Silva-Junior, E.B. (No Conflict); Silva-Gonçalves, A. J. (No Conflict); Oliveira, M.P. (No Conflict); Covre L.P. (No Conflict); Oliveira-Gomes, D.C. (No Conflict); Da-Cruz, A. M. (No Conflict); da Fonseca-Martins, A.M. (No Conflict); de Matos Guedes, H. L. (No Conflict).

ABSTRACT

Mucosal Leishmaniasis is one of the most aggressive clinical manifestations of *Leishmania* infection disease, characterized by the destruction of nasal and oral tissues. The mechanisms by which this disease occurs are still not well understood due to the lack of effective experimental models. Mucosal leishmaniasis is associated with inflammatory response, especially Th17 response. Based on that, in this work, the immunopathological aspects of the experimental infection of BALB/c mice by *Leishmania amazonensis* in the mucosa site were evaluated due to high susceptibility and the disease been associated with Th17 response. Three infection modes were performed and compared according to the injection site. Six weeks post infection, mice presented edema in the nasal and premaxillary region, with progressive growth until twelve weeks. The micro–Computerized Tomography and the histology images demonstrated that the parasite inoculation led to destruction of squamous and transitional tissues in NC and NB groups, with several cells harboring amastigotes. Mice infected in the mucosa tissues had higher parasite load and IgG, IgM antibody levels and increased production of cytotoxic mediators such as CD107, granzyme b and perforin, inflammatory cytokines as IFN-γ and IL-17, but lower frequencies of $CD4^+$ $IL\text{-}10^+$ cells compared to ear dermis. Taken together, our data shows that *L. amazonensis* parasites are more proliferative in nasal mucosa and the infection leads to an increased inflammatory response compared to ear dermis, pointing to this model as an interesting approach to understand some features of MCL immunopathology.

Keywords: Leishmaniasis, Mucosa, *L. amazonensis*, BALB/c, Experimental Infection

Introduction

Leishmaniasis is a group of neglected tropical diseases caused by infection by protozoan parasites belonging to the genus *Leishmania*. The disease affects the most deprived populations in the world, being endemic in more than 98 countries, with cases distributed across Asia, Africa, the Middle East, and South and Central America [1]. Estimates suggest that around 1 million new cases of leishmaniasis occur every year globally, with a population of 1 billion people living in areas at risk of contracting the disease [2].Of the different clinical manifestations of leishmaniasis, mucocutaneous leishmaniasis (MCL) stands out because it can generate a severe deformity, generating destruction of the tissues of the nose, upper lips, palate, pharynx, larynx, perforation of the septum and loss of bone tissue [3, 4]. Mucocutaneous Leishmaniasis (MCL) is a consequence of *Leishmania*'s tropism for mucosal tissues, involving the respiratory mucosa of the upper tract and the oral cavity. This clinical manifestation is typically a result of infection with New World species such as *Leishmania braziliensis*, *Leishmania panamensis*, *Leishmania guyanensis* and *Leishmania amazonensis* [5]. It is estimated that 3 to 5% of cases of cutaneous leishmaniasis caused by these species evolve into the mucosal form [6]. The cure rate for MCL treatment is lower compared to LCL [7, 8], which highlights the importance of a better understanding of development and immune response in this clinical manifestation [9, 10].

Therefore, despite being a more severe manifestation and even with a wide range of *Leishmania* species that can cause MCL and capable of infecting small rodents such as hamsters and mice, there is a lack of experimental models for MCL [5], and the immune response associated with this clinical manifestation is still poorly characterized. Using *L. amazonensis* infection on BALB/c mice that is very susceptible to infection, we hypothesized that the parasite could establish the infection directly to the nose inducing a manifestation similar to mucosal leishmaniasis. Previous attempts were made in the literature using subcutaneous infection in the paw leading to mucosal metastasis,

however, they are very long (approximately 8 months after infection) diverse (some animals do not develop the disease) and several mice don't survive during the prolonged infection and aging process. It is urgent a model that facilitates the study of mucosal leishmaniasis [11]. In the context of the disease, mucosal leishmaniasis is associated with a Th1, but also a Th17, neutrophil infiltrate immune response [12]. Meanwhile, BALB/c dermal pathology is associated with Th2 [13] but also with a strong Th17 [14, 15], making BALB/c a model to exploit the role of those immune axis to the pathology of mucosal leishmaniasis. In this way, here in we established a *L. amazonensis* mucosal leishmaniasis mice model using three infections sites to understand the immunopathology of the disease.

Methods

Leishmania Culture

In this work, parasites of the species *L. amazonensis* (MHOM/BR/75/JOSEFA) were used. The promastigotes were maintained in 25cm² culture flasks with M199 medium (pH 7.2), supplemented with 10% fetal bovine serum, 5µg/mL bovine hemin, 50U/mL penicillin, and 50µg/mL streptomycin.

Animals

Mice from BALB/c lineage, females aged 8-12 weeks, were used. The mice came from the Biotério Central de Camundongos of the Centro de Ciências da Saúde (CCS) from the Universidade Federal do Rio de Janeiro, mice were maintained under the Protocol of the Ethics Committee on the Use of Experimental Animals No. 133/23 of the CCS.

Infection and Lesion Development

The parasites were cultivated until the beginning of the stationary phase. The culture containing the promastigote forms were collected, washed with phosphate buffer

saline (PBS); and centrifuged for 10 minutes at 4°C at 1000 x G force. After centrifugation, the supernatant was discarded, and the cells were washed with PBS. The procedure was repeated twice. Then the cells were counted and adjusted to a concentration of $2x10^8$ parasites/mL. The animals were sedated with ketamine and xylazine and infected with $2x10^6$ parasites using Hamilton® syringes coupled with 34G needles. Different infection methods were implemented: intradermal in the ear performed at an angle of 20°; Cutaneous Nose, with the inoculum carried out at the apex of the mouse's nose; Septum, with the inoculum occurring in the mouse septum and “Nasobasal”, with the inoculum being carried out at an angle of 60° towards the lower “floor” part of the nose. The lesion was monitored with photos. Weekly measurements of the mice's ears were taken using Mitutoyo™ thickness gauges.

Micro Computerized Tomography, 3D Reconstruction e Lesion Analysis

Animals were sedated and placed in the LabPET8 Flex Triumph Gamma Medica™ tomography system at CENABIO, UIPA. The equipment settings included 60kV, 480µA, 1024 projections, 8-minute acquisition, and 30x magnification with a 39.46mm field of view, focusing on the snout and mucous membrane. After acquisition, data was reconstructed and analyzed using 3D Slicer™ software, with the Scissors tool applied to generate the snout area.

Histology Analysis

Tissues from animal snouts were fixed in 4% formaldehyde in PBS for 15 days. Decalcification was performed for 28 days using 10% EDTA. After fixation and decalcification, tissues were dehydrated through a series of ethanol and xylene solutions, then embedded in paraffin. Sections (5µm thick) were cut, rehydrated, and stained with Hematoxylin & Eosin (H&E). Tissue processing was done by the Histotechnology Platform at IOC - FIOCRUZ. Histology was performed with n = 5 per group.

Parasite Load Quantification

At the end of each experiment, parasite load was assessed using the limiting dilution method (LDA). Animals were euthanized with an overdose of Ketamine and Xylazine, and tissues (snout, nose tip, cheek, ear, spleen, NALT, auricular and cervical lymph nodes) were collected, weighed, and macerated in 1mL of M199. Serial 1:4 dilutions were made, and the results were plotted. Three experiments (n=3-5) were conducted, with two examining the entire snout and one focusing on segmented parts, 12 weeks post-infection.

Flow Cytometry

Flow cytometric analysis of cells from cervical and ear lymph nodes of infected or naïve animals was performed. Tissues were macerated, and cells counted with 0.1% trypan blue dye. $1x10^6$ cells were plated in a 96-well plate, centrifuged, and stimulated with PMA (20ng/mL), ionomycin (1µg/mL), and monensin (2.5µg/mL) in Complete RPMI for 4 hours at 37°C. Cells were blocked with anti-FcR, surface stained, fixed using the eBioscience™ FoxP3 kit, and intracellularly labeled. The samples were analyzed on a BD LSR Fortessa X-20 cytometer. Table S1 denotes the cytometer configuration. Table S2 shows the antibodies (BioLegend™) used and their concentrations. Figure S1 denotes the performed gating strategy.

Statistics

Results are represented by Standard Error of the Mean (SEM). Statistical significance was performed by unpaired two tailed Student t test with 95% confidence interval ($p<0,05$) for the respective data: Lesion profile by tomography, parasite load quantification and cytometry. While One Way ANOVA with 95% interval of confidence ($p<0,05$) was performed using Tukey post-test, for the ELISA OD Sum data. Statistically significant differences were defined as * for $p<0,05$; ** for $p<0,005$; *** for $p<0,0005$.

Results

Direct inoculation of *Leishmania amazonensis* in nasal mucosa led to injury but the lesion profile depends on the type of inoculum performed.

To assess *Leishmania* infection in the nasal mucosa, $2x10^6$ promastigotes of *L. amazonensis* were directly inoculated into different nasal sites of mice. After 6 weeks, the Nose Cutaneous (NC) and Nasobasal (NB) groups developed visible lesions with edema and redness (figure 1A). These lesions progressed and became necrotic by 12 weeks in some cases. The muzzle volume was significantly larger in the NC and NB groups ($387mm^3$ and $616mm^3$) compared to the Sham group (figure 1B), resembling the progressive ear infection, which reached 1.8mm in thickness (figure 1C, 1D). In contrast, the Septum group showed no visible lesions throughout the study (figure 1A). These results indicate that nasal inoculation can cause tissue damage, depending on the infection site.

The Nasal mucosa model showed a higher parasite load than ear dermis infection.

Parasite load in infected mice ranged from 10^6 to 10^8 parasites per gram of tissue in the Nose Cutaneous (NC) and Nasobasal (NB) groups, while the Septum (ST) group showed only 10^4 parasites, with Only 20% of animals testing positive (Figure 2A). Ear dermis infections had 10^6 parasites per gram (Figure 2B). Parasites were mostly concentrated in the edema sites, such as the nose tip and pre-maxillary regions (Figures 2C, 2D). Some animals in the NB group had around 10^5 parasites in NALT (Figure 2E). Only one animal in the NC group showed spleen infection (Figure 2F). The cervical lymph nodes of NC and NB mice had 10^6 parasites (Figure 2G), while the ear lymph nodes had 10^5 parasites (Figure 2H). The Septum group showed parasitic load in the cervical lymph node but not the nasal cavity (Figure 2G). These results indicate that mucocutaneous *L. amazonensis* infection leads to a higher parasite content in nasal mucosa infection compared to ear dermis, with the cervical lymph node being the primary draining node.

Nasal infection induced nasal swelling, but no septum perforation or new nasal cavity formation took place.

MicroCT analysis was performed to assess nasal cavity impairment, focusing on the NC and NB groups, as the ST group showed no visible lesions or significant parasite load. NC-infected mice typically had lesions at the nose apex, while NB-infected mice had lesions affecting the mucosa and premaxilla, extending to the upper lips (Figure 3A, 3B). No nasal cavity enlargement, perforations, or deformation were observed compared to controls (Figure S2), but tissue swelling was evident in both NC and NB groups (Figures 3A-D). Axial sections showed noticeable edema on the outer nasal cavity (Figure 3C, 3D). These results indicate that lesion profiles depend on the inoculation site, mainly affecting the nasal tissues initial portions.

Nasal infection promoted destruction and deconfiguration of squamous and transitional tissues.

Histological analysis of the nasal cavity revealed significant inflammation and parasite presence. In the NC group, edema with a neutrophilic infiltrate and vacuolated macrophages containing amastigotes was observed (Figure 3E, S3), along with respiratory epithelium loss (Figure S4B), and parasitized macrophages near cartilage (Figure S4E). In the NB group, similar edema and neutrophil infiltration were seen, with many parasitized macrophages (Figure 3F). Respiratory epithelium showed slight morphological changes, including cellular stress and detachment (Figure S4C, S4F). These findings indicate that *Leishmania* infection impacts the inner nasal mucosa in this model.

Nasal mucosa infection produced higher systemic antibodies titters compared to ear dermis infection.

To assess immune responses to different nasal mucosa infections by *Leishmania*, we measured antibody levels. The NC group showed the highest IgM, IgG,

and IgG1 levels, followed by NB and ED (Figure 4A-F). IgG2a and IgG2b were highest in NB, then NC (Figure 4G-J). Overall, NC and NB had stronger antibody responses than ED, while ST had the lowest. These findings suggest mucocutaneous infection triggers a stronger humoral response than ear dermis infection, with antibody profiles varying by inoculation site.

Cytotoxic and effector CD4$^+$ and CD8$^+$ T cells from draining lymph nodes were increased in NC, however, CD4$^+$ T cells producing IL-10 were impaired in nasal mucosa infection.

Flow cytometry of draining lymph nodes showed reduced CD4+ T cell frequency in the ED group but not in nasal infections. The NC and NB groups had increased total CD4+ T cells (Figure 5A) and higher numbers of cells expressing cytotoxic markers (CD107a, granzyme B, perforin) across NC, NB, and ED groups (Figures 5B-D), despite unchanged frequencies (Figures S6-S8).

Although frequencies remained unchanged (Figures S9-S10), total IFN-γ+ (Figure 5F) and IL-17+ (Figure 5G) cells increased in NC, NB, and ED groups. CD4+ IL-10+ T cells increased only in the ED group (Figure 5H), with lower IL-10-producing CD4+ T cell frequencies in nasal infections compared to ED (Figure 6A, B), highlighting distinct expansion dynamics between nasal and dermal infections.

We analyzed whether changes in CD4+ IL-10+ T cells were linked to CD4+ CD25+ FoxP3+ Tregs. Treg numbers increased in NC, NB, and ED groups without frequency changes (Figure S11). Similar trends were observed for CD25- FoxP3+, CD25+ FoxP3-, and CD25- FoxP3- cells (Figures S12-14), indicating the IL-10 reduction is unrelated to regulatory T cell frequency.

We also analyzed CD8$^+$ T lymphocytes during mucosal infections. NC and NB groups showed an expansion in total CD8$^+$ T cells (Figure 7A) with frequencies similar

to $CD4^+$ T cells (Figure S15). Cytotoxic $CD8^+$ T cells markers increased in NC, NB, and ED groups (Figures 7B-D), with NC showing higher $CD8^+$ $Perforin^+$ frequency (Figure S18), nut no frequency changes to CD107a and Granzyme B respectively (figure S16, S17). There were no IFN-γ^+ $CD8^+$ significant changes in frequency (Figure 7F) or number (Figure S19). IL-17^+ $CD8^+$ T cells increased in NB and ED groups (Figure 7F) without frequency changes (Figures S20). $CD8^+$ IL-10^+ T cells showed no numerical change (Figure 7H), but frequency decreased in mucosa-infected and ED groups (Figure S21).

Discussion

Mucocutaneous Leishmaniasis (MCL) causes severe tissue damage in nasal, oral, and pharyngeal mucosa, leading to edema and erythema in affected areas [3, 5]. In our mouse model, the NC and NB groups developed visible edema and erythema by week 6, progressing over time. Lesions in the NC group formed at the nose tip and extended dorsally, resembling the experimental mucosal leishmaniasis in dogs and hamsters [16, 17]. In the NB group, lesions spread to the upper lips and premaxilla, mimicking clinical features of human MCL [18, 19].

Some animals developed necrotic lesions after 12 weeks of infection. While *L. amazonensis* typically causes non-necrotizing lesions in BALB/c mice resembling diffuse cutaneous leishmaniasis in humans [20]. Similar variation in infection sites was observed with *Leishmania major* [21], possibly linked to site-specific microbiota. Nasal microbiota, including *Staphylococcus* and *Streptococcus* species [22, 23], may exacerbate tissue damage by recruiting neutrophils and CD8 IL-17+ cells during infection [24, 25].

Mucosal leishmaniasis in humans often affects septa, cartilage, and nasal cavities, with occasional bone destruction visible via computed tomography [3, 26–28]. In this study, microCT revealed edema in the nasal and premaxilla regions of NC and NB groups. Histopathology showed dense cellular infiltrates and infected cells near

cartilage and the nasal mucosa, with respiratory epithelium changes, consistent with previous findings [11].

Despite MCL caused by *L. braziliensis* typically shows fewer parasites at the site than cutaneous leishmaniasis [29], our model NC and NB groups had higher parasite loads, including in draining lymph nodes and infected macrophages in nasal mucosa. This may reflect *L. amazonensis* characteristics, which produce higher parasite loads than *L. braziliensis* in mice [30] as evidenced also by the the cases o MCL caused by *L. amazonensis*, where parasite amastigotes were described as easily visualized in H&E sections [31]. Unlike previous models focusing on nasal infection [16, 17, 32, 33], this study uniquely examined infections within the nasal mucosa cavity, revealing that the inoculum site significantly influences lesion severity and parasite load across NC, ST, and NB groups. Necrosis was observed in some animals, a feature absents in other models [16, 17, 33]. Mucosal infections showed clinical aspects similar, or more severe than cutaneous ear lesions, aligning with findings in *L. panamensis*-infected hamsters [17]. While other models required approximately 8 months to develop lesions [11], this approach shortened progression to 6–8 weeks. Future studies could compare axenic amastigote infections, given their higher virulence and differing proliferation kinetics from promastigotes [34, 35].

MCL severity correlates with higher anti-*Leishmania* IgG levels [36]. In our model, mucosal infections (NC and NB) produced more IgM and IgGs than dermal infections, with NC favoring IgG1 (Th2 response) and NB favoring IgG2a (Th1 response). This highlights site-dependent immune response differences, consistent with established antibody production dichotomy [37], and the high antibody levels produced by the mucosal infection compared to dermis can be interpreted as an increased inflammatory response that may contribute to the severity of pathology.

To compare nasal mucosa infections with human MCL, we performed flow cytometry on lymph node cells. Mucosal infection (NC and NB) increased CD4+ and

CD8+ T cells expressing cytotoxic markers (CD107a, Granzyme B, Perforin) and IL-17, with less IFN-γ, but no increase in IL-10-expressing cells, unlike the ED group. In MCL, CD4+ T cells produce high IFN-γ and TNF-α, with elevated Th17 responses that recruit neutrophils and cause tissue damage [12, 38, 39]. MCL also shows higher granzyme A-expressing cells, linked to greater damage [34], with a lower IL-10 receptor expression, despite normal IL-10 expression [39]. Our data suggests a similar imbalance between cytotoxic and regulatory responses, with reduced IL-10+ cells and increased IL-17+ cells potentially contributing to severity, as IL-10 limits Th17-mediated pathology [40].

Taken together, *L. amazonensis* infection in BALB/c mice induces an immune response that reflects some aspects of the human MCL, with increased cytotoxic and effector cells but a compromised regulatory response. However, our studies didn't show some MCL features like cavity formation, septal perforations, and bone destruction, possibly due to parasite species or host lineage differences, or the shortened pathology compared to human pathology [28]. To address this, ongoing research is being performed with C57BL/6 strain for a stronger Th1 response [15, 41]. We also are planning to test the *L. braziliensis* hamster model for its higher susceptibility for this species [42]. As NC and NB sites differed in some characteristics, we believe that the combination of those inoculum sites may better represent the full mucosal leishmaniasis profile in mice. More studies are needed to confirm the lymphocyte profile in the mucosal site.

In conclusion, when infected directly at mucosal site, *L. amazonensis* parasites are more proliferative in nasal mucosa and lead to an increased cytotoxic and antibody response compared to ear dermis infection, which can be associated with the IL-10 impairment in the nasal mucosa that can be related to the immunopathology of MCL.

Author Contribution

Investigation: Alisson Amaral da Rocha[1,2], Júlio Souza dos Santos[1,2]; Alessandra Márcia da Fonseca Martins[1,2]; Igor Bittencourt dos Santos[1,2]; Douglas Barroso de Almeida[1,2]; João Victor Paiva Romano[1,2]; Naiara Carla dos Santos Manhães[1,2]; Hozany Praxedes dos Santos[1,2]; Marcia Pereira de Oliveira Duarte[4]; Antônio José da Silva Gonçalves[4].

Formal Analysis: Alisson Amaral da Rocha[1,2]; Alessandra Márcia da Fonseca-Martins[1,2] Elias Barbosa[3]

Conceptualization and Methodology: Alisson Amaral da Rocha[1,2], Júlio Souza dos Santos[1,2] Herbert Leonel de Matos Guedes[1,2]

Resources: Herbert Leonel de Matos Guedes[1,2], Alessandra Márcia da Fonseca-Martins[1,2], Alda Maria da Cruz[4], Daniel Claudio de Oliveira Gomes[5], Luciana Polaco Covre[5],

Writing – Original Draft: Alisson Amaral da Rocha[1,2]

Supervision and Funding Acquisition: Herbert Leonel de Matos Guedes[1,2]

Financial Support

This work was supported by Fundação de Amparo à Pesquisa Estado do Rio de Janeiro – FAPERJ and Coordenação de Aperfeiçoamento Pessoal do Ensino Superior – CAPES; Conselho Nacional de Desenvolvimento Científico e Tecnológico – CNPq.

Acknowledgement

We would like to acknowledge the Centro Nacional de Bioimagem (CENABIO) for the equipment and technical support in tomography analysis. We would also like to acknowledge the Platform of Histotechnology (FIOCRUZ-RJ) for the processing of histology samples.

Figures

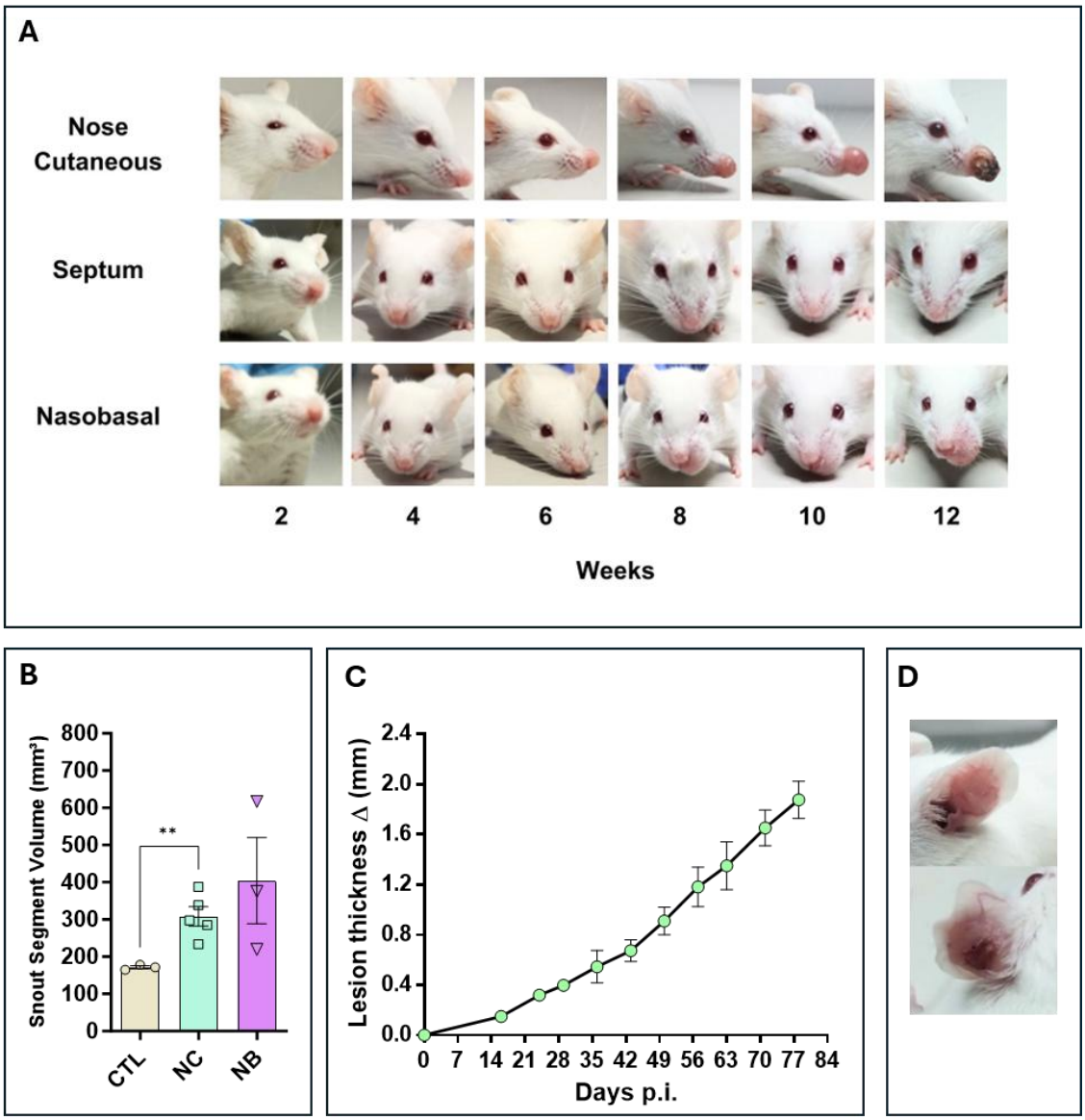

Figure 1. Nasal mucosa lesion profile. The modes of nasal mucosa inoculation with *L. amazonensis*. Nose cutaneous (NC) group was inoculated in the nostril nose dermis; Septum (ST) was inoculated in the septum tissue, "Nasobasal" (NB) was inoculated in the nasal floor. In all cases was used an 34G needle. **(A)** Lesion profile of the three groups, during a period of 12 weeks post infection (p.i), showing a continuous development of edema and erythema starting at 6 to 8 weeks for the NC and NB group. ST group does not show any sign of lesion. **(B)** Snout volume quantification 12 weeks p.i (Standard Error of the Mean – (SEM)), using micro–Computerized Tomography (micro-CT). NC and NB groups have greater volume compared to control groups. **(C)** Ear dermis lesion thickness of mice infected in the ear as an infection control group (SEM). The thickness continuous increases during the experiment reaching around 2.0mm in 12 weeks p.i. **(D)** Representative ear of a mice from control infection group showing edema and erythema.

(B) Representative data of 3 independent experiments (5 animals per group). (C) Data from one experiment 3-5 animals per group. (D) Representative data from 2 independent experiments 5 animals were used. Statistics: unpaired t-test * $p < 0.05$.

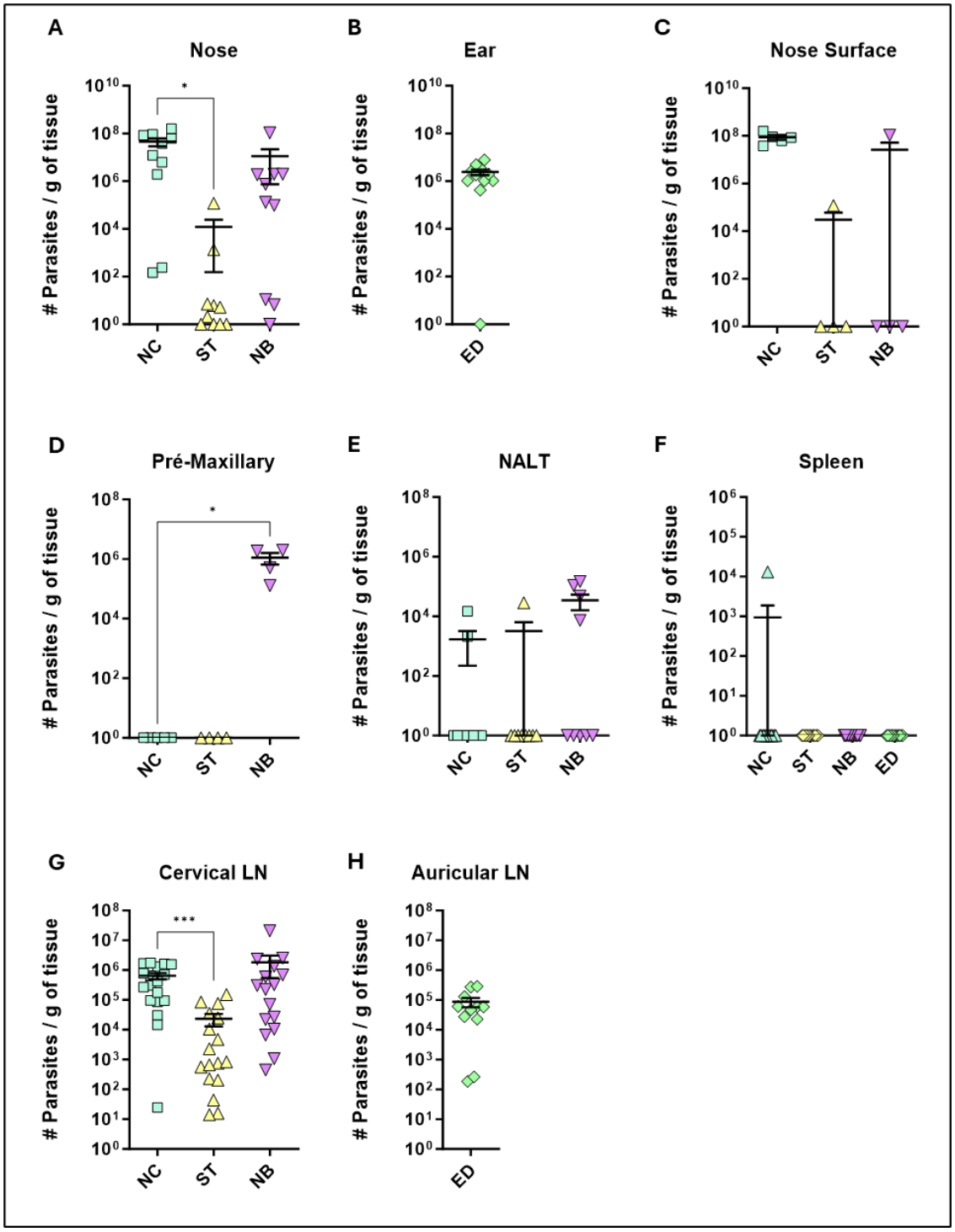

Figure 2. Parasite Load Profile. Profile of parasite load per gram of tissue, of the different groups of infection. NC, ST, NB, ED means respectively to Nose Cutaneous, Septum, "Nasobasal" and Ear dermis infection groups. The following tissues are represented in the figure: **(A)** Nose = the entire snout containing

the nasal tissues; **(B)** Ear; **(C)** Nose Surface = only the visible nose; **(D)** mice premaxillary region; **(E)** Nasal Associated Lymphoid Tissue (NALT); **(F)** Spleen; **(G)** Cervical lymph node; **(H)** auricular lymph node. Parasite load was detected by the limiting dilution method (LDA) carried out at the end of the experiment (approximately 12 weeks of infection).

(A) Data from 3 independent experiments; (B, C, and D) 1 independent experiment; and (E), Data from 4 independent experiments; (G and H), 2 independent experiments. N = 5 animals per group. Data represented by the Standard Error of The Mean (SEM). Statistics: unpaired t-test * $p < 0.05$.

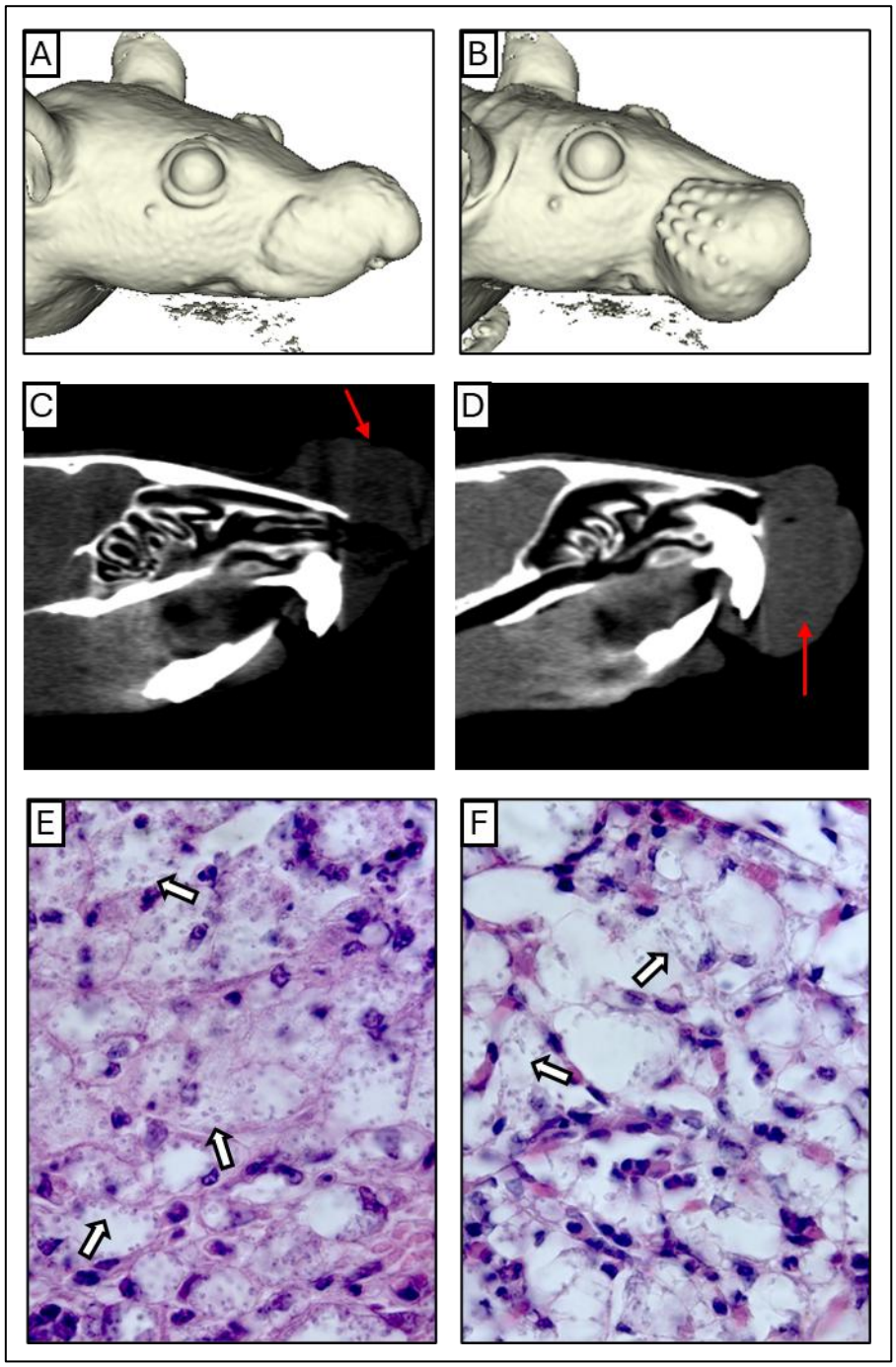

382 **Figure 3. Anatomical and Histological Profile. (A, B)** A complete three-dimensional reconstruction
383 of NC and NB mice model respectively. **(C, D)** Coronal Section planes showing edema and partial
384 nose obstruction of NC and NB mice respectively. **(E, F)** Intense inflammatory infiltrate containing
385 infected cells, below the epithelium of NC and NB mice respectively. The red arrows indicate the region
386 of edema, and the white arrows show examples of cells bearing amastigotes. Magnification: E) 1000x and
387 (F) 1000x.

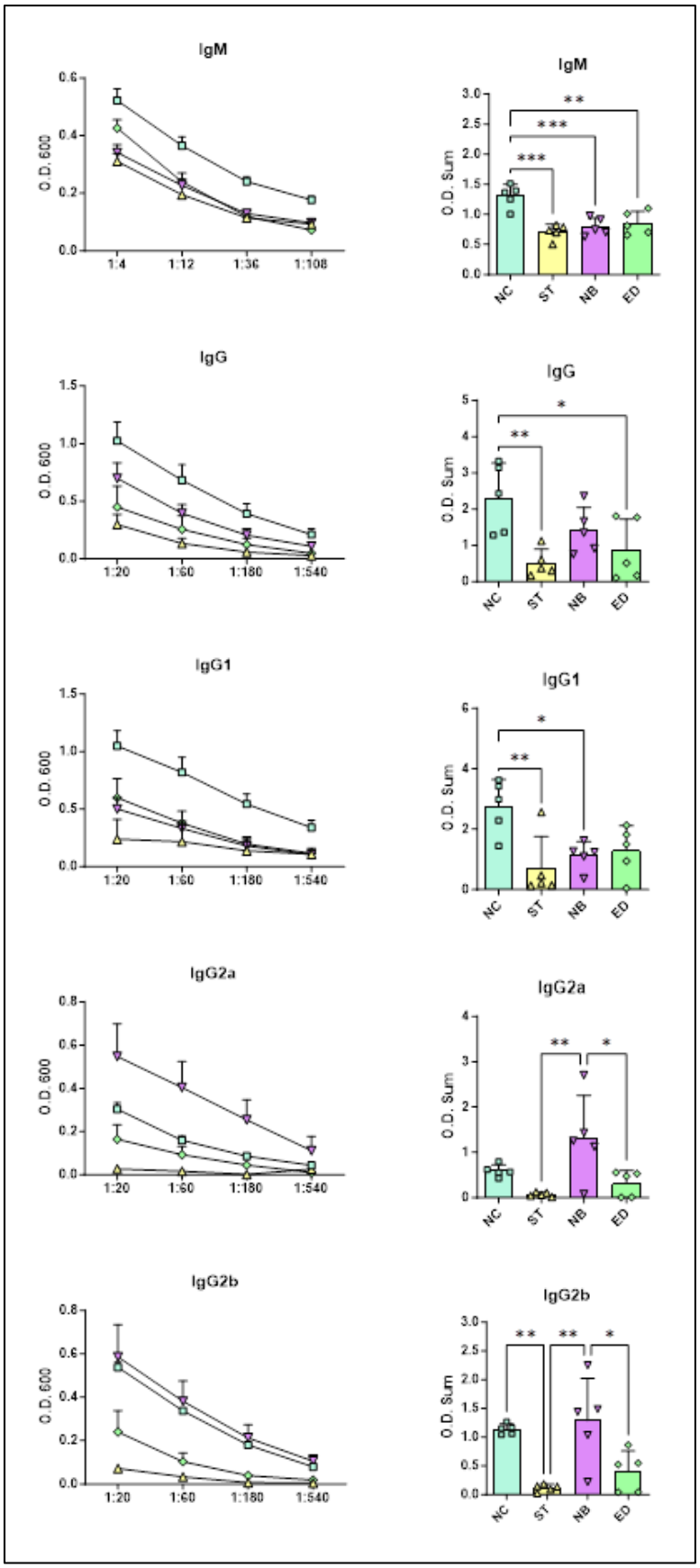

Figure 4: Systemic antibodies infection profile. Systemic antibodies responses in the different infected groups. **(A, C, E, G)** Ig titration using four dilutions, represented by O.D. 600 absorbance measurements

(Standard Error of The Mean (SEM)). **(B, D, F, H)** Ig O.D. Sum from each animal and groups. NC groups produce more IgM, total IgG and IgG1, while NB mode of infection have more IgG2a and IgG2b. NC, ST, NB, ED groups represented by square; triangle; inverse triangle and diamond respectively. Statistics: One-way ANOVA; * p<0,05; ** p<0,005; ***p<0,0005.

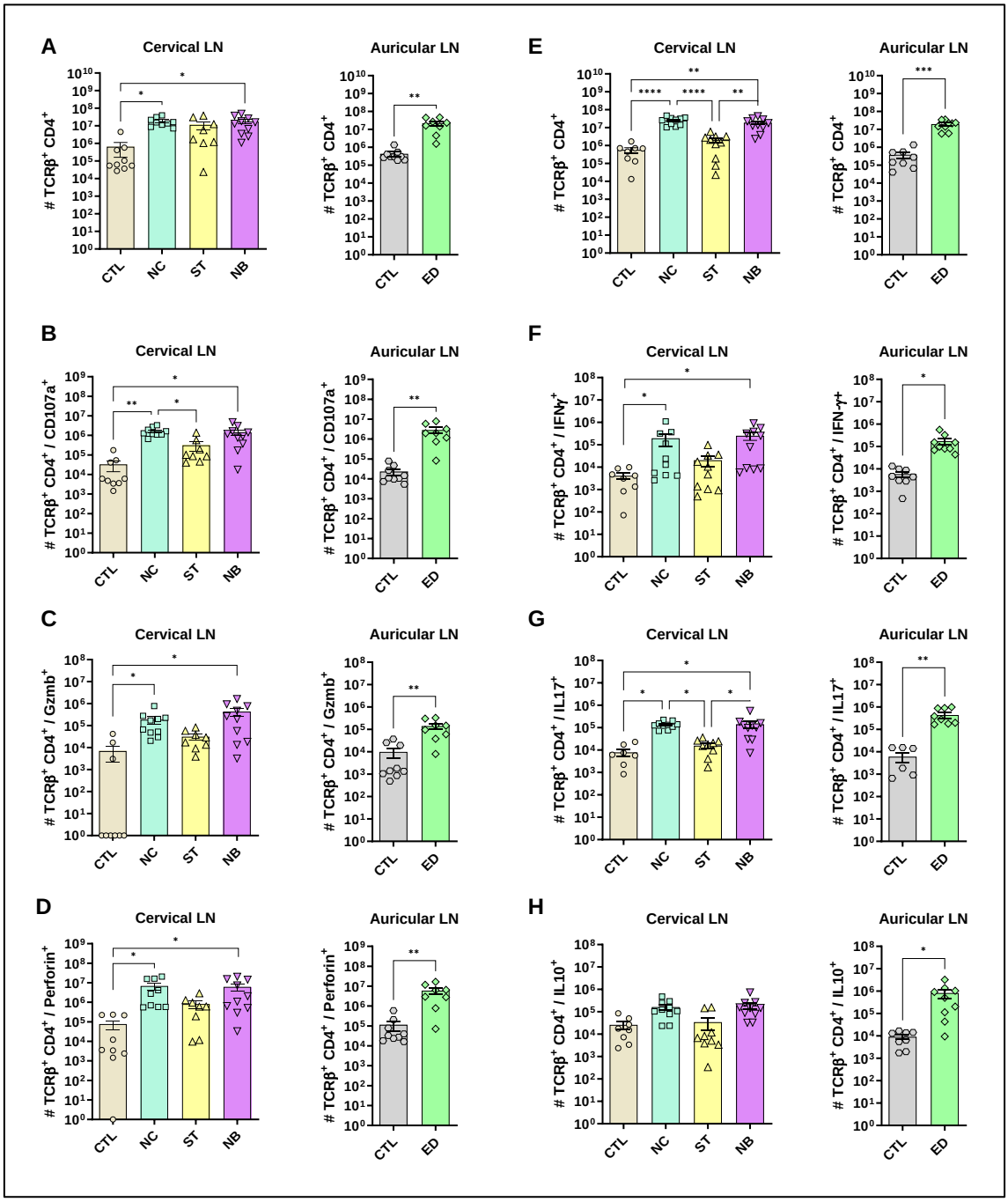

Figure 5. CD4⁺ T cells cytotoxic and effector profile. (A-D) The cytotoxic profile of T helper lymphocytes was measured by the expression of CD107a, Granzyme B and Perforin. (A) Cervical and auricular lymph nodes total Lymphocytes counts are shown in logarithmic scale; (B) total cells expressing CD107a, (C) Granzyme B; (D) Perforin. (E-H) The effector profile of T helper lymphocytes was measured by the

expression of IL-10, IL-17 and IFN-γ. (E) Cervical and auricular lymph nodes total lymphocytes counts are shown in logarithmic scale; (F) total cells expressing IFN-γ, (G) IL-17; (H) IL-10. Data accumulative of two independent experiments (3-6 animals per group). Statistics: plot with Standard Error of The Mean (SEM), t-test was used for all groups and samples * p<0,05, **<0,005.

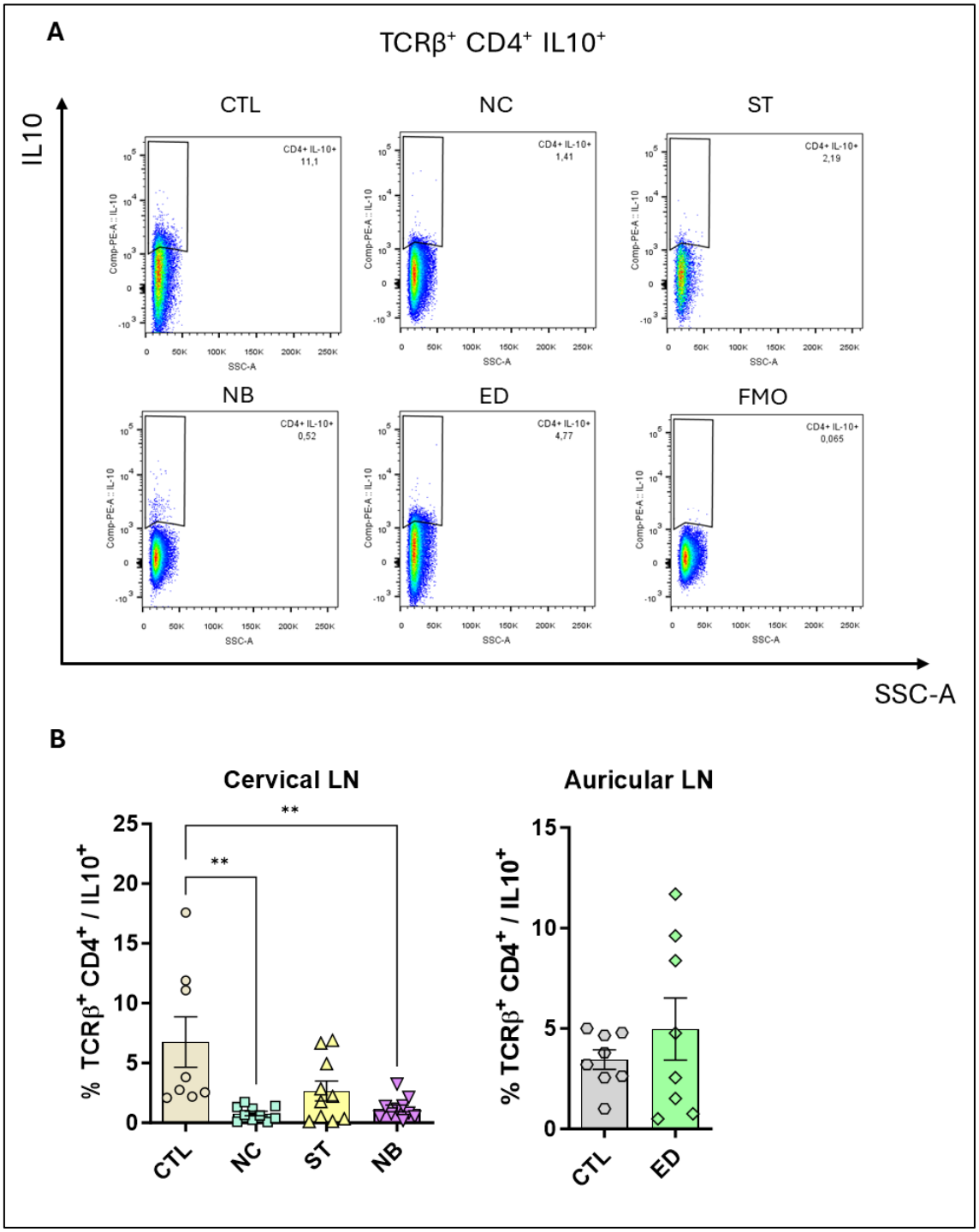

Figure 6. CD4⁺ T cells IL-10⁺ is impaired. The IL-10 producing CD4⁺ T cells was measured, and the frequency is shown. (A) Pseudocolor dot plot showing the representative animals of each group. (B) Frequency plot from cervical and auricular lymph nodes from infected animal vs controls. Data accumulative of two independent experiments (3-6 animals per group). Statistics: plot with Standard Error of The Mean (SEM), t-test was used for all groups and samples * p<0,05, **<0,005.

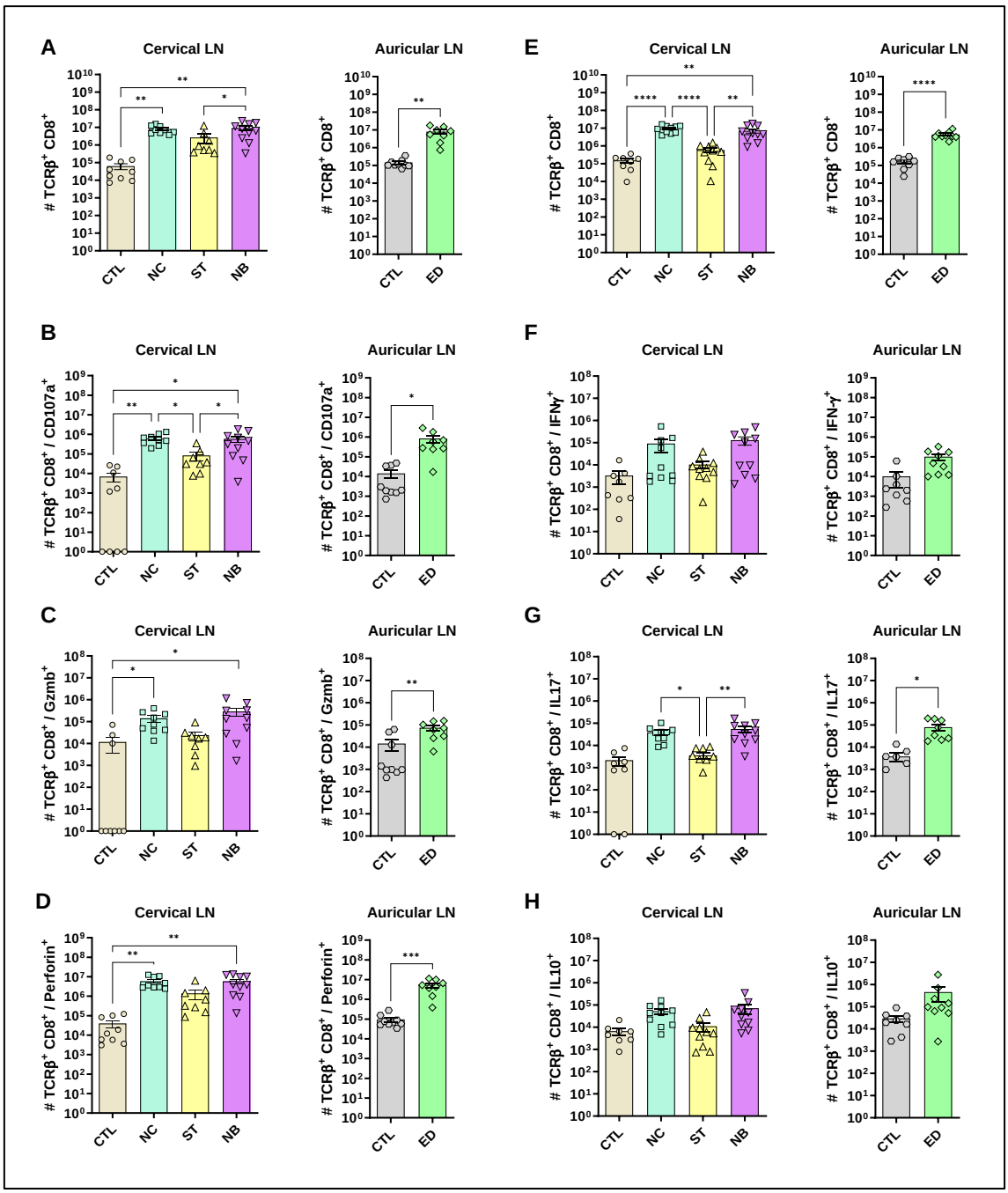

Figure 7. Cytotoxic and effector profile of CD8⁺ T cells. (A-D) The cytotoxic profile of T helper lymphocytes was measured by the expression of CD107a, Granzyme B and Perforin. (A) Cervical and auricular lymph nodes total Lymphocytes counts are shown in logarithmic scale; (B) total cells expressing CD107a, (C) Granzyme B; (D) Perforin. (E-H) The effector profile of T helper lymphocytes was measured by the expression of IL-10, IL-17 and IFN-γ. (E) Cervical and auricular lymph nodes total lymphocytes counts are shown in logarithmic scale; (F) total cells expressing IFN-γ, (G) IL-17; (H) IL-10. Data accumulative of two independent experiments (3-6 animals per group). Statistics: plot with Standard Error of The Mean (SEM), t-test was used for all groups and samples * p<0,05, **<0,005, ***<0,0005.

Reference list

1. Mann S, Frasca K, Scherrer S, et al. A Review of Leishmaniasis: Current Knowledge and Future Directions. Current Tropical Medicine Reports [Internet]. **2021**; 8(2):1–12. Available from: https://www.ncbi.nlm.nih.gov/pmc/articles/PMC7966913/

2. World Health Organization. Leishmaniasis [Internet]. Who.int. World Health Organization: WHO; 2022. Available from: https://www.who.int/news-room/fact-sheets/detail/leishmaniasis

3. Lessa MMi, Lessa HA, Castro TWN, et al. Mucosal leishmaniasis: epidemiological and clinical aspects. Brazilian Journal of Otorhinolaryngology. **2007**; 73(6):843–847.

4. Goto H, Lindoso JAL. Cutaneous and Mucocutaneous Leishmaniasis. Infectious Disease Clinics of North America. **2012**; 26(2):293–307.

5. Strazzulla A, Cocuzza S, Pinzone MR, et al. Mucosal Leishmaniasis: An Underestimated Presentation of a Neglected Disease. BioMed Research International [Internet]. **2013**; 2013. Available from: https://www.ncbi.nlm.nih.gov/pmc/articles/PMC3703408/

6. Handler MZ, Patel PA, Kapila R, Al-Qubati Y, Schwartz RA. Cutaneous and mucocutaneous leishmaniasis: Clinical perspectives. Journal of the American Academy of Dermatology [Internet]. **2015**; 73(6):897–908. Available from: https://www.jaad.org/article/S0190-9622(14)01914-8/fulltext

7. Cincurá C, Lima CMF de, Machado PRL, et al. Mucosal leishmaniasis: A Retrospective Study of 327 Cases from an Endemic Area of Leishmania (Viannia) braziliensis. The American Journal

of Tropical Medicine and Hygiene [Internet]. **2017** [cited 2023 Mar 29]; 97(3):761–766. Available from: https://www.ncbi.nlm.nih.gov/pmc/articles/PMC5590558/

8. Martins SS, Barroso DH, Rodrigues BC, et al. A Pilot Randomized Clinical Trial: Oral Miltefosine and Pentavalent Antimonials Associated With Pentoxifylline for the Treatment of American Tegumentary Leishmaniasis. Frontiers in Cellular and Infection Microbiology [Internet]. **2021** [cited 2023 Feb 7]; 11:700323. Available from: https://pubmed.ncbi.nlm.nih.gov/34277476/

9. Sampaio RNR, Silva JSF e, Paula CDR de, et al. A randomized, open-label clinical trial comparing the long-term effects of miltefosine and meglumine antimoniate for mucosal leishmaniasis. Revista da Sociedade Brasileira de Medicina Tropical. **2019**; 52.

10. Calvopina M, Jijon S, Serrano E, Kato H. Case Report: Successful Treatment with Miltefosine of Severe New World Mucosal Leishmaniasis Caused by Leishmania guyanensis. The American Journal of Tropical Medicine and Hygiene. **2020**; 103(2):752–755.

11. Cupolilo SM, Souza F, Abreu-Silva AL, Calabrese KS, Goncalves C. Biological behavior of Leishmania (L.) amazonensis isolated from a human diffuse cutaneous leishmaniasis in inbred strains of mice. PubMed. National Institutes of Health; **2003**; 18(4):1059–65.

12. Boaventura V, Santos CS, Ribeiro C, et al. Human mucosal leishmaniasis: Neutrophils infiltrate areas of tissue damage that express high levels of Th17-related cytokines. European Journal of Immunology. Wiley-Blackwell; **2010**; 40(10):2830–2836.

13. Sacks, D., Noben-Trauth, N. The immunology of susceptibility and resistance to *Leishmania major* in mice. *Nat Rev Immunol* **2**, 845–858 (2002). https://doi.org/10.1038/nri933

14. Lopez Kostka S, Dinges S, Griewank K, Iwakura Y, Udey MC, von Stebut E. IL-17 promotes progression of cutaneous leishmaniasis in susceptible mice. J Immunol. 2009 Mar 1;182(5):3039-46. doi: 10.4049/jimmunol.0713598. PMID: 19234200; PMCID: PMC2658650.

15. Dos-Santos JS, Firmino-Cruz L, Ramos TD, et al. Characterization of Sv129 Mice as a Susceptible Model to Leishmania amazonensis. Frontiers in Medicine. **2019**; 6.

16. Pirmez C, Marzochi MCA, Coutinho SG. Experimental canine mucocutaneous leishmaniasis (Leishmania braziliensis braziliensis). Memórias do Instituto Oswaldo Cruz. **1988**; 83(2):145–151.

17. Osorio Y, Melby PC, Pirmez C, Chandrasekar B, Guarín N, Travi BL. The site of cutaneous infection influences the immunological response and clinical outcome of hamsters infected with *Leishmania panamensis*. Parasite Immunology. Wiley-Blackwell; **2003**; 25(3):139–148.

18. Marsden PD. Mucosal leishmaniasis due to Leishmania (Viannia) braziliensis L(V)b in Três Braços, Bahia-Brazil. Revista da Sociedade Brasileira de Medicina Tropical. **1994**; 27(2):93–101.

19. Lambertucci JR, Coulaud R, Cristina L. Mucosal leishmaniasis. Revista Da Sociedade Brasileira De Medicina Tropical. Brazilian Society of Tropical Medicine; **2003**; 36(2):307–308.

20. Pérez H, Arredondo B, González M. Comparative study of American cutaneous leishmaniasis and diffuse cutaneous leishmaniasis in two strains of inbred mice. Infection and Immunity. **1978**; 22(2):301–307.

21. Baldwin TM, Elso C, Curtis J, Buckingham L, Handman E. The Site of *Leishmania major* Infection Determines Disease Severity and Immune Responses. Infection and Immunity. American Society for Microbiology; **2003**; 71(12):6830–6834.

22. Bomar L, Brugger SD, Lemon KP. Bacterial microbiota of the nasal passages across the span of human life. Current Opinion in Microbiology. **2018**; 41:8–14.

23. Thangaleela S, Sivamaruthi BS, Kesika P, Bharathi M, Chaiyasut C. Nasal Microbiota, Olfactory Health, Neurological Disorders and Aging—A Review. Microorganisms. **2022**; 10(7):1405.

24. Borbón TY, Scorza BM, Clay GM, et al. Coinfection with Leishmania major and Staphylococcus aureus enhances the pathologic responses to both microbes through a pathway involving IL-17A. Dutra WO, editor. PLOS Neglected Tropical Diseases. **2019**; 13(5):e0007247.

25. Singh TP, Carvalho AM, Sacramento LA, Grice EA, Scott P. Microbiota instruct IL-17A-producing innate lymphoid cells to promote skin inflammation in cutaneous leishmaniasis. Stäger S, editor. PLOS Pathogens. **2021**; 17(10):e1009693.

26. Rojas-Jaimes J, Lescano AG, Frischtak HL, Arenas J. Case Report: Mucosal Leishmaniasis Presenting with Nasal Septum Perforation after Almost Thirty Years. The American Journal of Tropical Medicine and Hygiene. **2018**; 99(2):327–330.

27. Bhowate RR, Bhargava PA, Badki SD, Mrunal Meshram. Mucosal Leishmaniasis Involving the Nostril and Maxillary Sinus: A Case Report. Cureus. Cureus, Inc.; **2022**;

28. Camargo RA de, Nicodemo AC, Sumi DV, et al. Facial Structure Alterations and Abnormalities of the Paranasal Sinuses on Multidetector Computed Tomography Scans of Patients with Treated Mucosal Leishmaniasis. PLOS Neglected Tropical Diseases. Public Library of Science; **2014**; 8(7):e3001–e3001.

29. Jara M, Adaui V, Valencia BM, et al. Real-Time PCR Assay for Detection and Quantification of Leishmania (Viannia) Organisms in Skin and Mucosal Lesions: Exploratory Study of Parasite Load and Clinical Parameters. Journal of Clinical Microbiology. **2013**; 51(6):1826–1833.

30. Carvalho Ak, Silveira Ft, Passero Lfd, Gomes Cmc, Corbett Cep, Laurenti Md. Leishmania (V.) braziliensis and L. (L.) amazonensis promote differential expression of dendritic cells and cellular immune response in murine model. Parasite Immunology. **2012**; 34(8-9):395–403.

31. Sampaio RN, Marsden PD, Cuentas EAL, Cuba CAC, Grimaldi Jr. G. Leishmania mexicana amazonensis isolated from a patient with fatal mucosal leishmaniasis. Revista da Sociedade Brasileira de Medicina Tropical. FapUNIFESP (SciELO); **1985**; 18(4):273–274.

32. Teva A, Porrozzi R, Cupolillo E, Pirmez C, Oliveira-Neto Mp, Grimaldi G. Leishmania (Viannia) braziliensis-induced chronic granulomatous cutaneous lesions affecting the nasal mucosa in the rhesus monkey (Macaca mulatta) model. Parasitology. **2003**; 127(5):437–447.

33. Cortes S, Esteves C, Maurício I, et al. *In vitro* and *in vivo* behaviour of sympatric *Leishmania (V.) braziliensis, L. (V.) peruviana* and their hybrids. Parasitology. **2011**; 139(2):191–199.

34. Mendes Costa D, Cecílio P, Santarém N, Cordeiro-da-Silva A, Tavares J. Murine infection with bioluminescent Leishmania infantum axenic amastigotes applied to drug discovery. Scientific Reports. **2019**; 9(1).

35. Baek K-H, Piel L, Rosazza T, Prina E, Späth GF, No JH. Infectivity and Drug Susceptibility Profiling of Different Leishmania-Host Cell Combinations. Pathogens. **2020**; 9(5):393.

36. Lima CMF de, Magalhães AS, Costa R, et al. High Anti-Leishmania IgG Antibody Levels Are Associated With Severity of Mucosal Leishmaniasis. Frontiers in Cellular and Infection Microbiology. **2021**; 11.

37. Bretscher PA. On the Mechanism Determining the Th1/Th2 Phenotype of an Immune Response, and its Pertinence to Strategies for the Prevention, and Treatment, of Certain Infectious Diseases. Scandinavian Journal of Immunology. **2014**; 79(6):361–376.

38. Bacellar O, Lessa HA, Schriefer A, et al. Up-Regulation of Th1-Type Responses in Mucosal Leishmaniasis Patients. **2002**; 70(12):6734–6740.

39. Faria DR, Gollob KJ, BarbosaJ, et al. Decreased In Situ Expression of Interleukin-10 Receptor Is Correlated with the Exacerbated Inflammatory and Cytotoxic Responses Observed in Mucosal Leishmaniasis. Infection and Immunity. **2005**; 73(12):7853–7859.

40. Gonzalez-Lombana C, Gimblet C, Bacellar O, et al. IL-17 Mediates Immunopathology in the Absence of IL-10 Following Leishmania major Infection. Langhorne J, editor. PLoS Pathogens. **2013**; 9(3):e1003243.

41. Tomiotto-Pellissier F, Milena Menegazzo Miranda-Sapla, Taylon Felipe Silva, et al. Murine Susceptibility to Leishmania amazonensis Infection Is Influenced by Arginase-1 and Macrophages at the Lesion Site. Frontiers in Cellular and Infection Microbiology. Frontiers Media; **2021**; 11.

42. Gomes-Silva A, Nogueira RDS, Amato VS, et al. Can interferon-γ and interleukin-10 balance be associated with severity of human *Leishmania (Viannia) braziliensis* infection?. Clinical and Experimental Immunology. Oxford University Press; **2007**; 149(3):440–444.

Supplementary Material

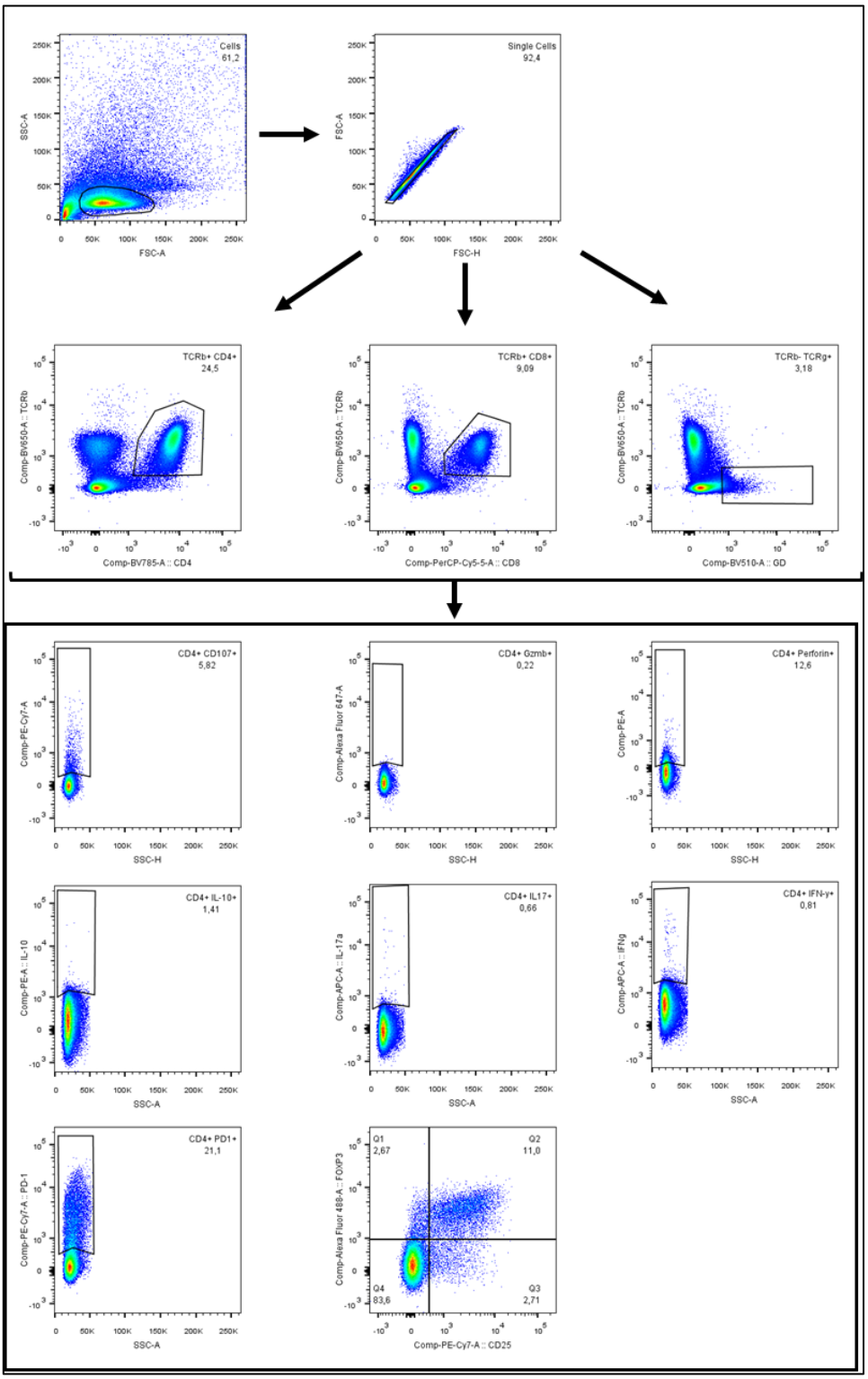

Figure S1. Gating strategy. The figure shows the gating strategy used to find and analyze CD4⁺ T, CD8⁺ T and Tγδ⁺ T cells. Within each population, a gate was performed to highlight cells

547 expressing the molecules CD107a, Perforin, Granzyme B, IL10, IL17 and IFN-γ (except Tγδ⁺)
548 and PD-1. In CD4⁺ T cells, the concomitant expression of CD25 and FoxP3 was also verified.

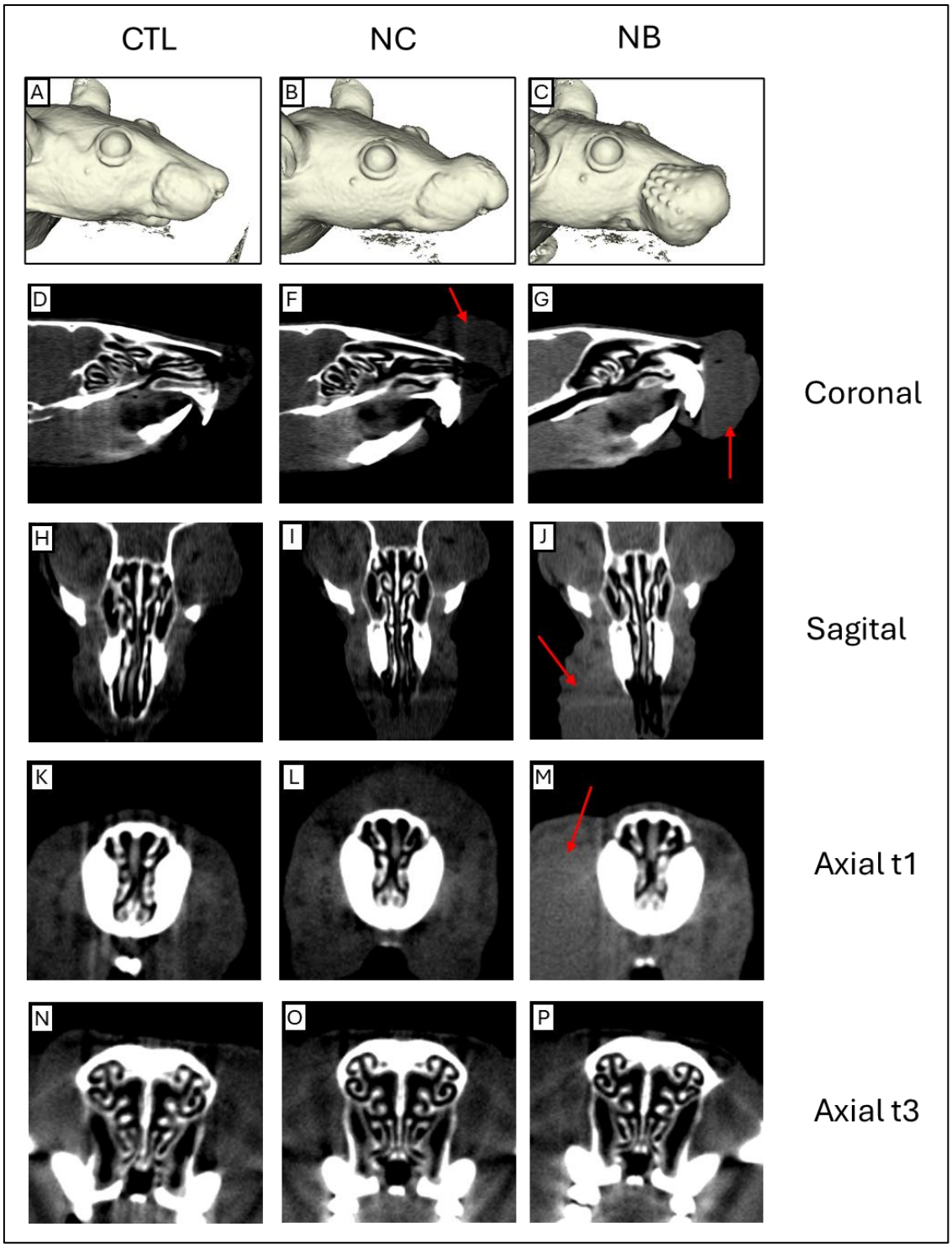

549

550 **Figure S2. Small animal computed tomography (microCT).** The complete three-dimensional
551 reconstructions of the mice (first row). The microCT of the Control (CTL) mock PBS injection in
552 the three sites, Nose Cutaneous (NC) and Nasobasal (NB) groups is also shown, under different

553 section planes: Coronal, Sagittal and Axial at t1 and t3. The red arrows indicate the region of
554 edema. The group NC showed an edema in the nostril region that can progress to the upper part
555 of the snout (second column. While NB infection mode led to a progressive swelling of
556 premaxillary region (third column). No nasal cavity formation was observed, in any of the
557 segments and infection groups.

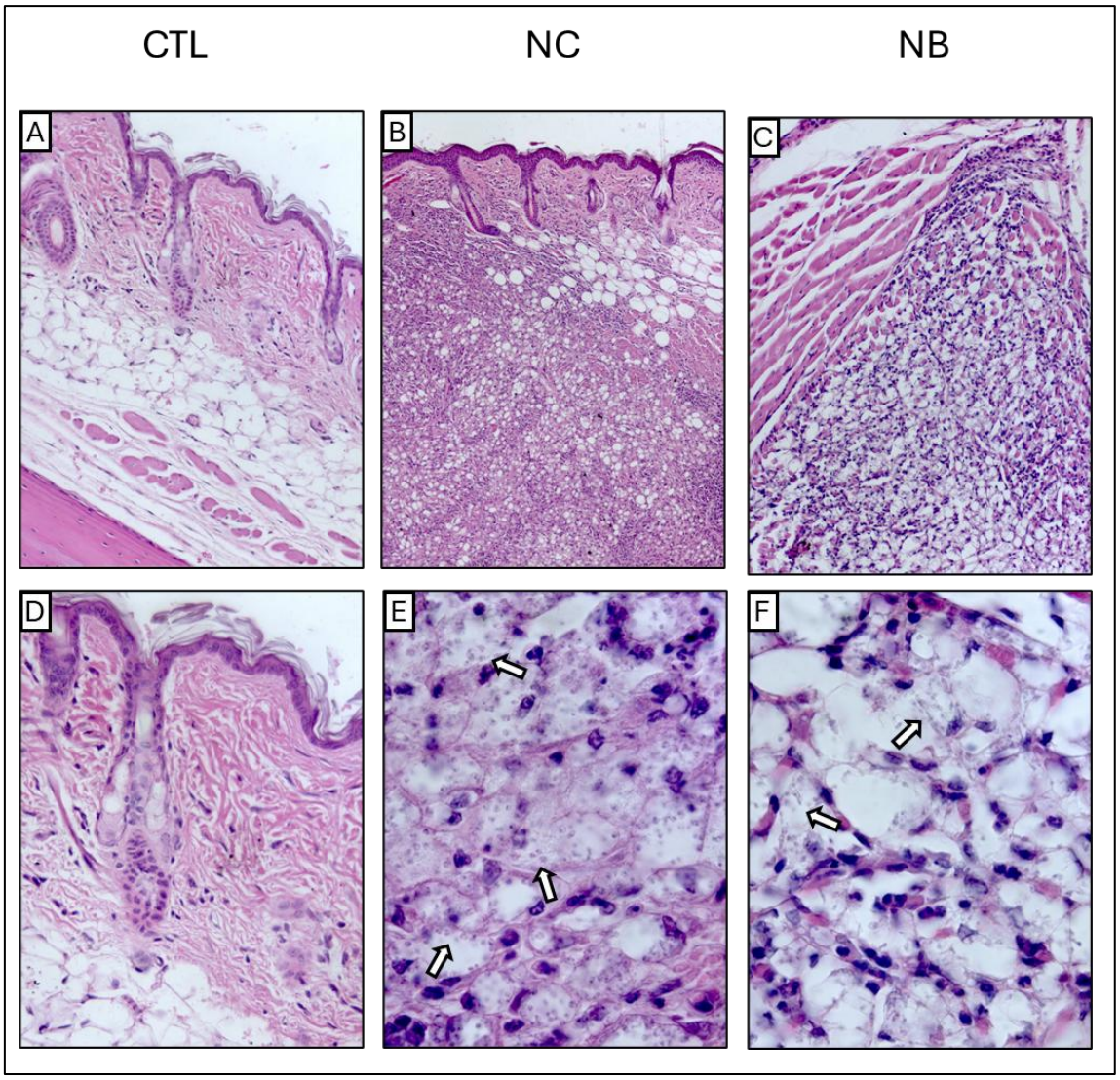

558

559 **Figure S3: Histopathological Sections of the Epidermal Region of the Nose.**
560 Histopathological appearance of the nasal skin tissue from the Control (CTL) mock PBS injection
561 in the three sites, Cutaneous Nose (NC) and Nasobasal (NB) groups, 12 weeks after the start of
562 the experiment, stained with hematoxylin and eosin (H&E). The animals were infected with $2x10^6$
563 parasites**. (A, D)** appearance of the dermis of control animals. **(B, E)** NC group showing
564 inflammatory infiltrate containing infected macrophages, below the epithelium. **(C, F)** NB group

565 showing intense inflammatory infiltrate with parasitized macrophages. Arrows shows examples of
566 macrophages bearing amastigotes. Magnification: (A) 200x; (B) 100x; (C) 100x; (D); 400x; (E)
567 1000x and (F) 1000x.

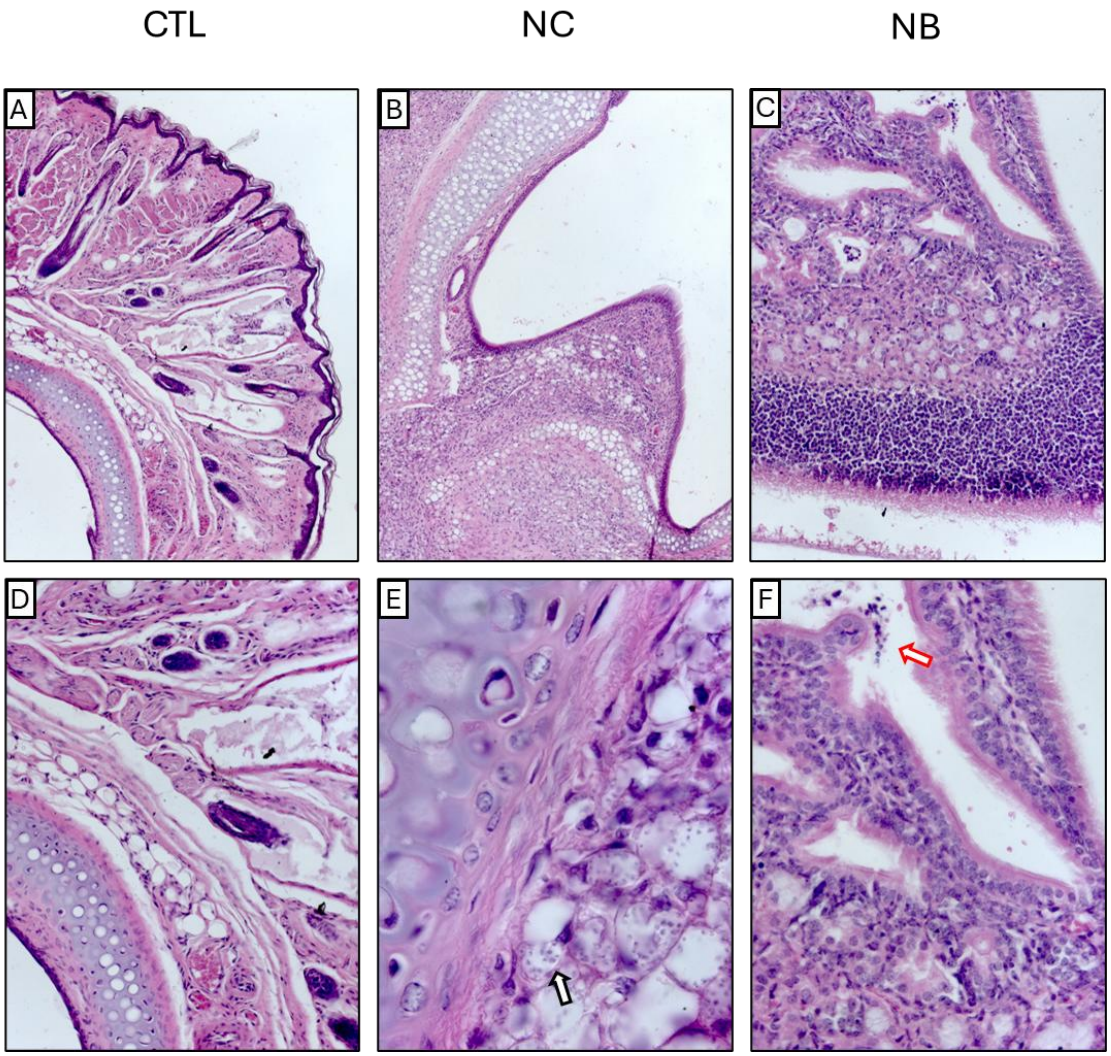

568

569 **Figure S4: Histopathological Sections of the Initial Internal Region (T1) of the Nasal**
570 **Mucosa.** Histopathological appearance of the nasal tissue from the Control (CTL) mock PBS
571 injection in the three sites, Cutaneous Nose (NC) and Nasobasal (NB) groups, 12 weeks after the
572 start of the experiment, stained with hematoxylin and eosin (H&E). The animals were infected
573 with $2x10^6$ parasites. **(A, D)** appearance of the dermis and squamous epithelium of control
574 animals. **(B, E)** NC group showing inflammatory infiltrate containing infected macrophages, close
575 to the cartilaginous regions. **(C, F)** NB group, demonstrating stress and structural disorganization
576 of the tissue accompanied by cell detachment. White arrows show examples of macrophages

bearing amastigotes, red arrows show example of cell detachment. Magnification: (A) 100x; (B) 100x; (C) 100x; (D); 200x; (E) 1000x and (F) 200x.

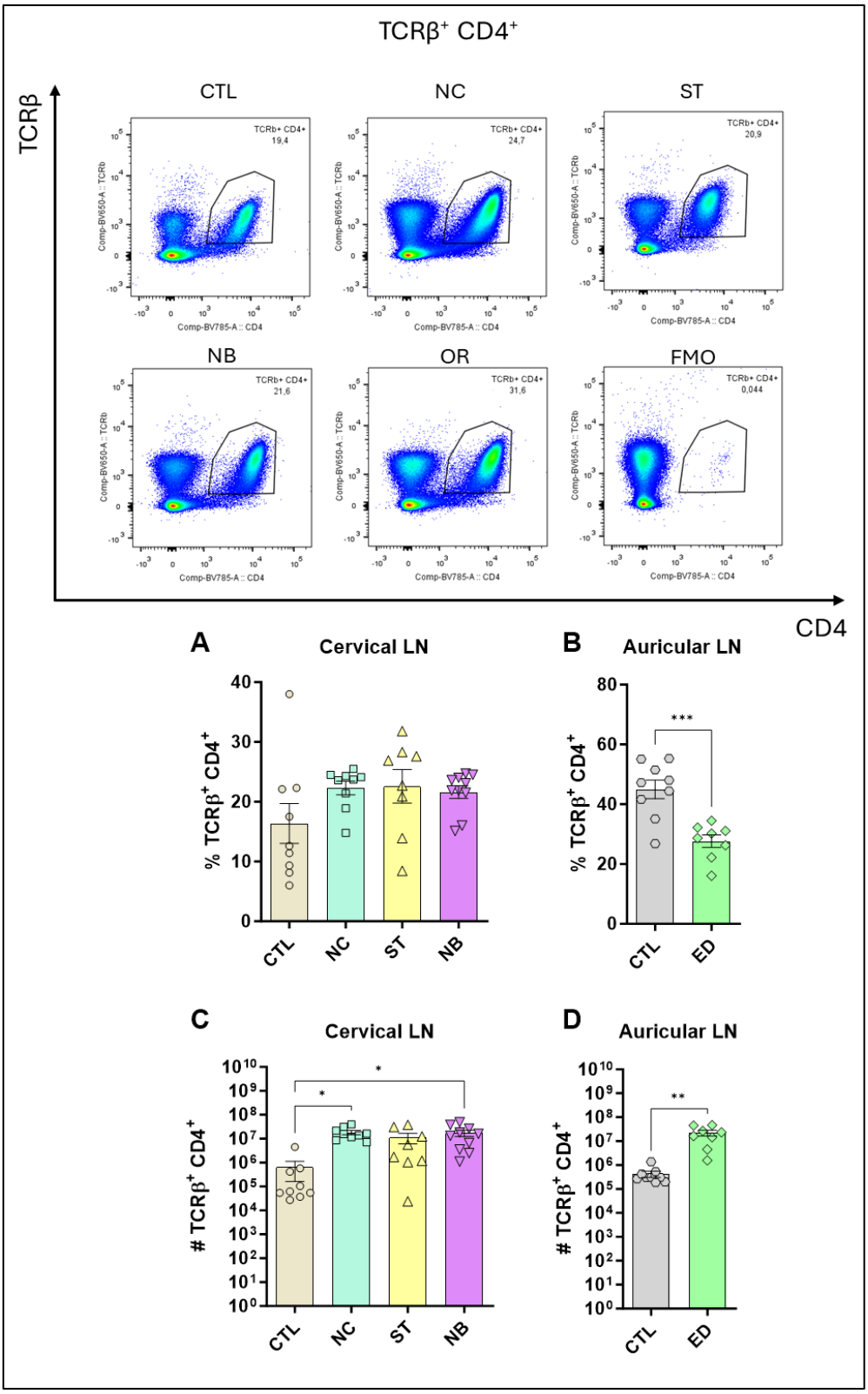

583

584 **Figure S5. Profile of TCRβ⁺ CD4⁺ Cells.** The figure shows the representatives and graphs with

585 the percentage of cells in the nasal and ear sites (A) and (B) respectively. In (C) and (D) data on

586 the total number of cells are represented. Data accumulative of two independent experiments.

587 Statistics: plot with Standard Error of The Mean (SEM), t-test was used for all groups and samples

588 * p<0,05, **<0,005., 3-6 animals per group in each.

589

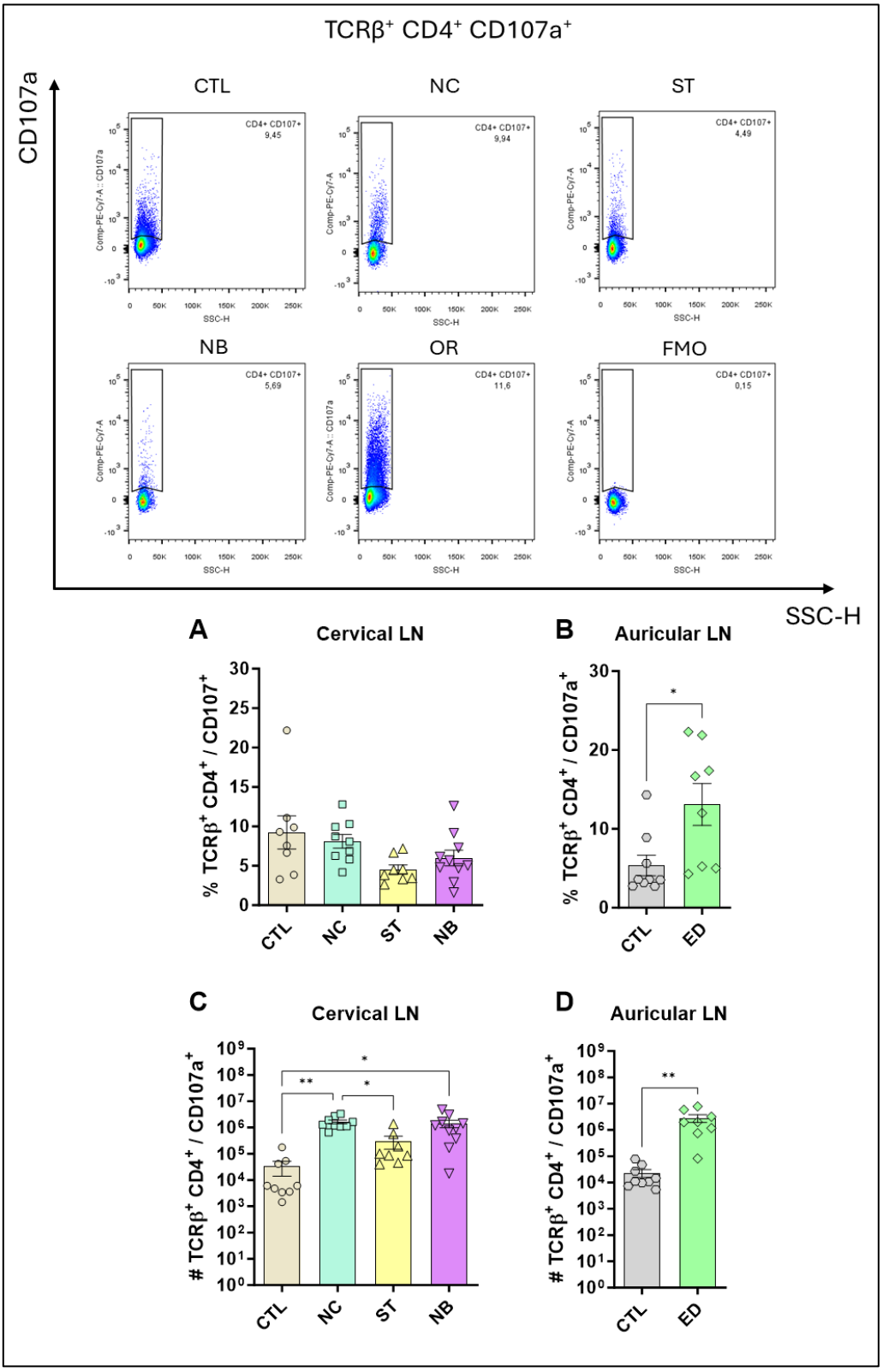

590

591 **Figure S6. Profile of TCRβ$^+$ CD4$^+$ CD107a$^+$ Cells.** The figure shows the representatives and
592 graphs with the percentage of cells in the nasal and ear sites (A) and (B) respectively. In (C) and
593 (D) data on the total number of cells are represented. Data accumulative of two independent
594 experiments. Statistics: plot with Standard Error of The Mean (SEM), t-test was used for all groups
595 and samples * p<0,05, **<0,005., 3-6 animals per group in each.

596

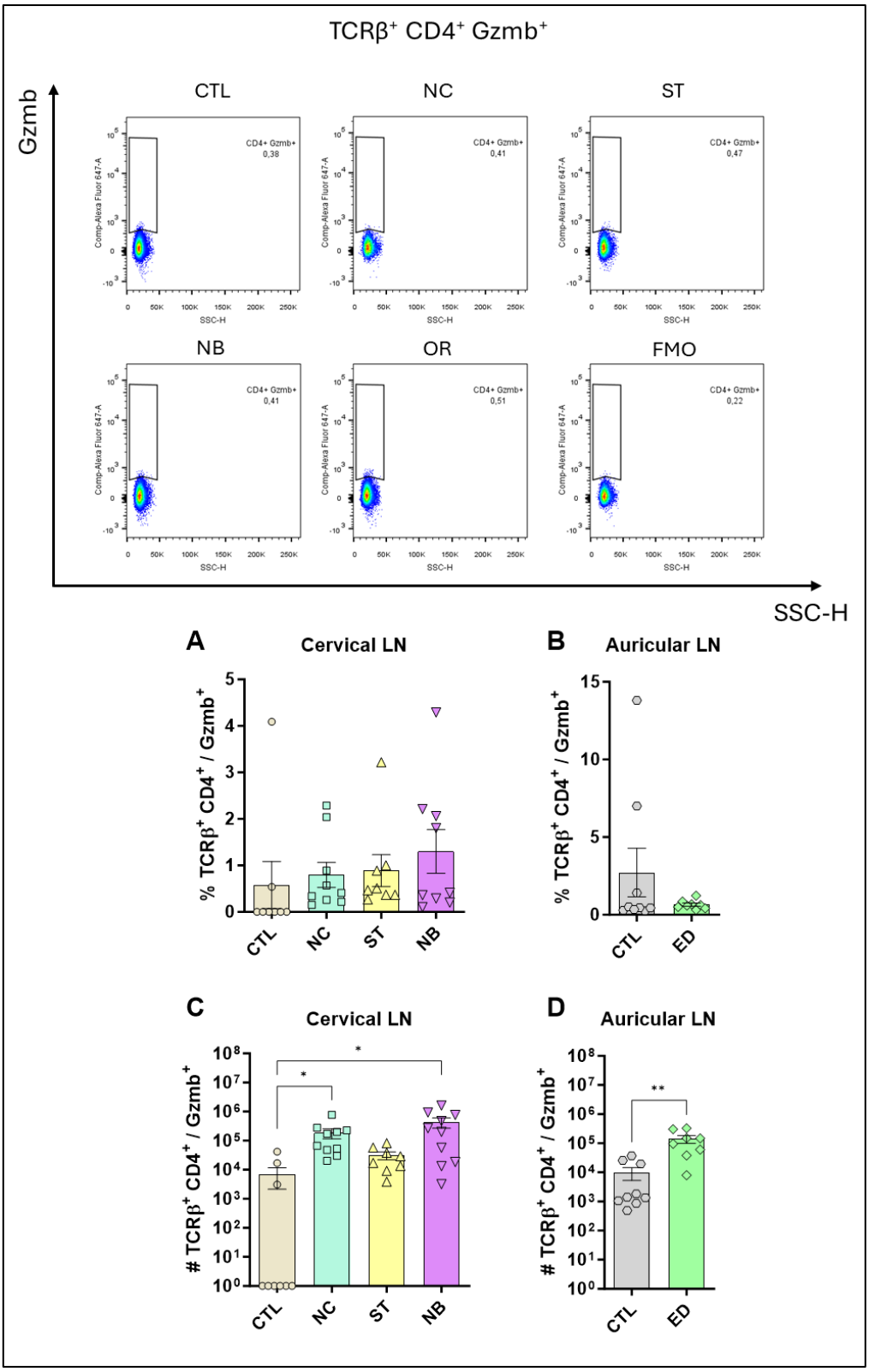

597

598 **Figure S7. Profile of TCRβ⁺ CD4⁺ Gzmb⁺ Cells.** The figure shows the representatives and
599 graphs with the percentage of cells in the nasal and ear sites (A) and (B) respectively. In (C) and
600 (D) data on the total number of cells are represented. Data accumulative of two independent

experiments. Statistics: plot with Standard Error of The Mean (SEM), t-test was used for all groups and samples * p<0,05, **<0,005., 3-6 animals per group in each.

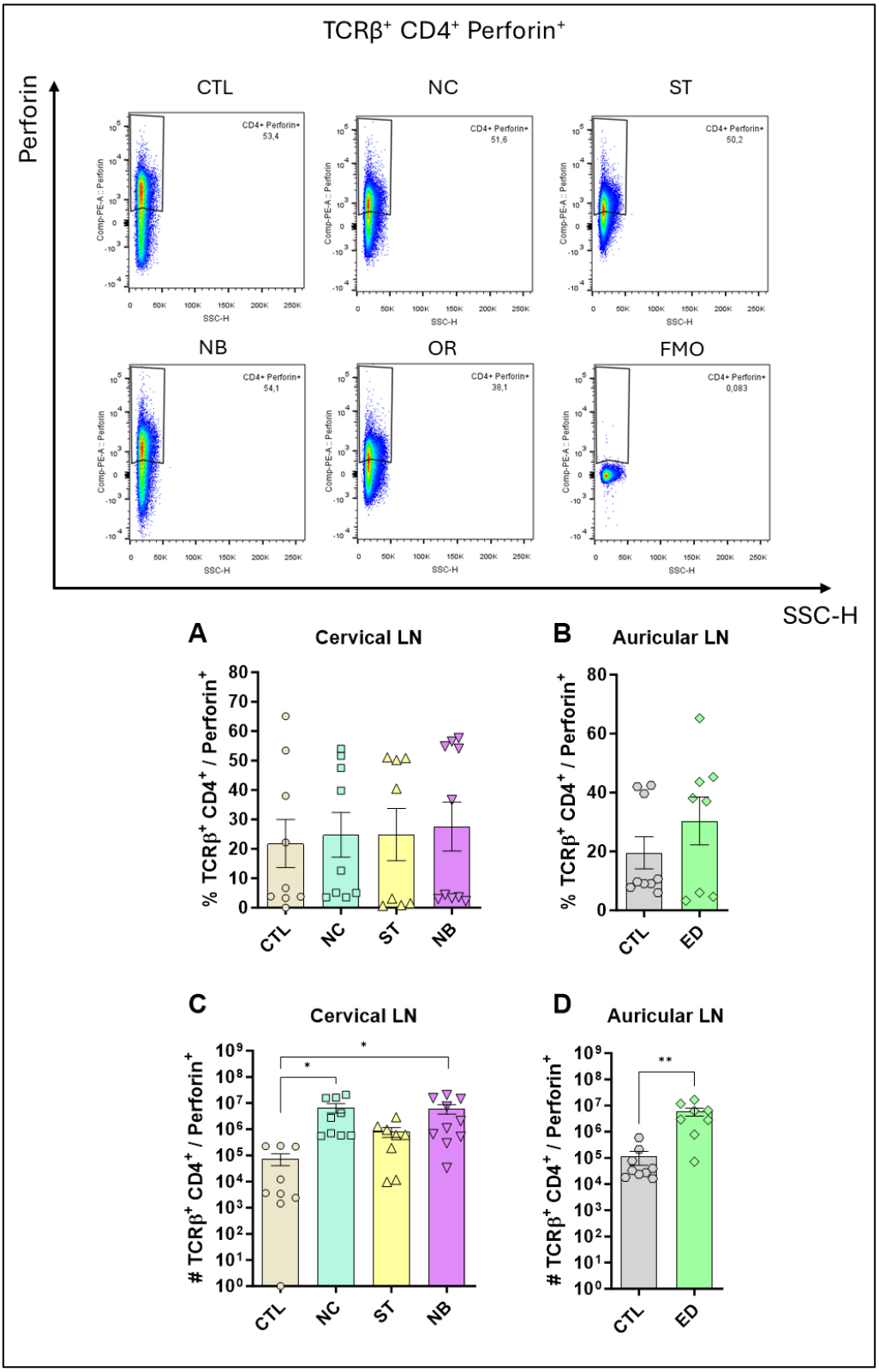

605 **Figure S8. Profile of TCRβ$^+$ CD4$^+$ Perforin$^+$ Cells.** The figure shows the representatives and
606 graphs with the percentage of cells in the nasal and ear sites (A) and (B) respectively. In (C) and
607 (D) data on the total number of cells are represented. Data accumulative of two independent
608 experiments. Statistics: plot with Standard Error of The Mean (SEM), t-test was used for all groups
609 and samples * p<0,05, **<0,005., 3-6 animals per group in each.

610

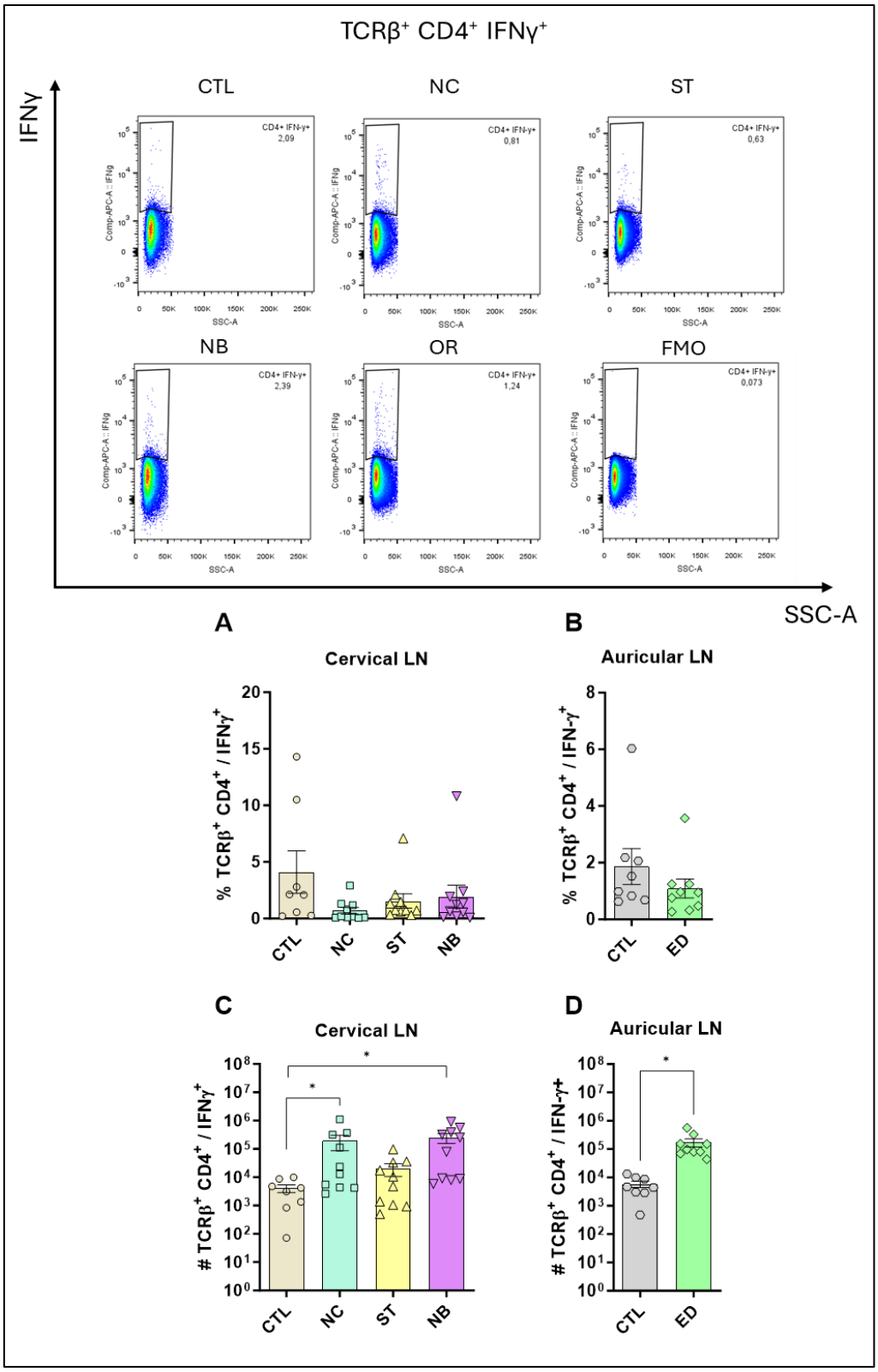

611

612 **Figure S9. Profile of TCRβ⁺ CD4⁺ IFN-γ⁺ Cells.** The figure shows the representatives and graphs

613 with the percentage of cells in the nasal and ear sites (A) and (B) respectively. In (C) and (D) data

614 on the total number of cells are represented. Data accumulative of two independent experiments.

Statistics: plot with Standard Error of The Mean (SEM), t-test was used for all groups and samples * p<0,05, **<0,005., 3-6 animals per group in each.

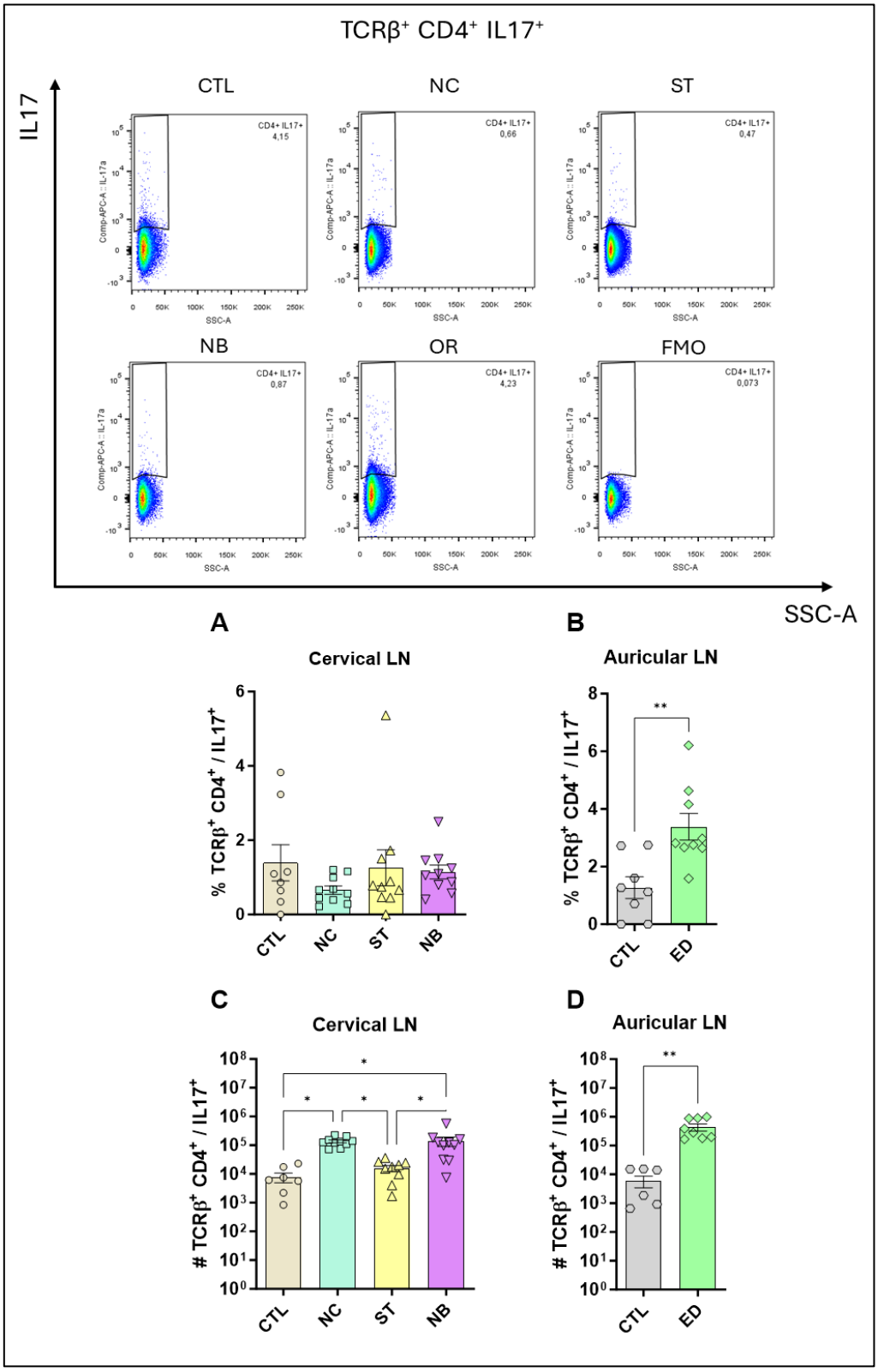

619 **Figure S10. Profile of TCRβ^{+} CD4^{+} IL-17^{+} Cells.** The figure shows the representatives and
620 graphs with the percentage of cells in the nasal and ear sites (A) and (B) respectively. In (C) and
621 (D) data on the total number of cells are represented. Data accumulative of two independent
622 experiments. Statistics: plot with Standard Error of The Mean (SEM), t-test was used for all groups
623 and samples * p<0,05, **<0,005., 3-6 animals per group in each.

624

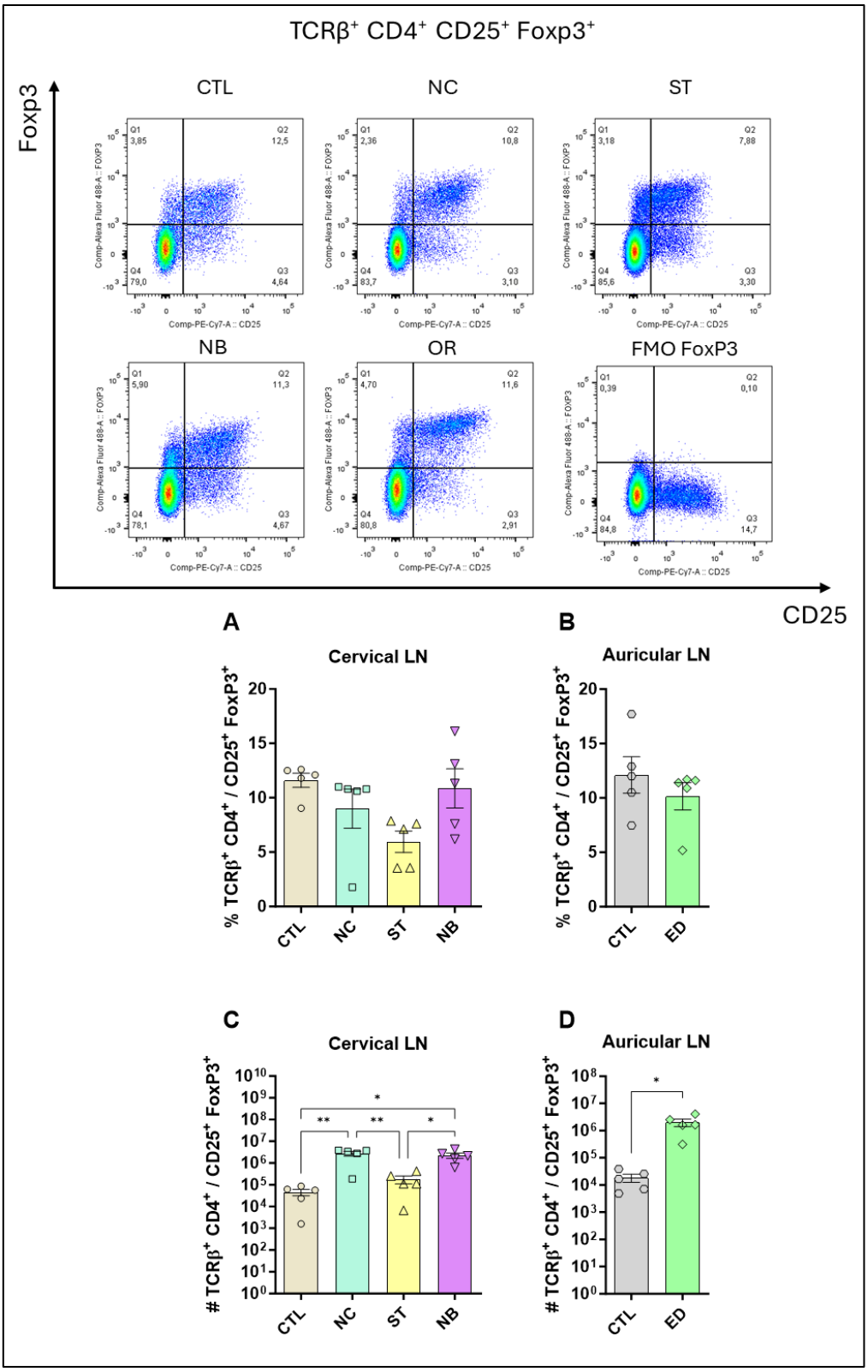

625

626 **Figure S11. TCRβ⁺ CD4⁺ CD25⁻ FoxP3⁺ profile.** The figure shows the representatives and
627 graphs with the percentage of cells in the nasal and ear sites (A) and (B) respectively. In (C) and
628 (D) data on the total number of cells are represented. Data accumulative of two independent

experiments. Statistics: plot with Standard Error of The Mean (SEM), t-test was used for all groups and samples * p<0,05, **<0,005., 3-6 animals per group in each.

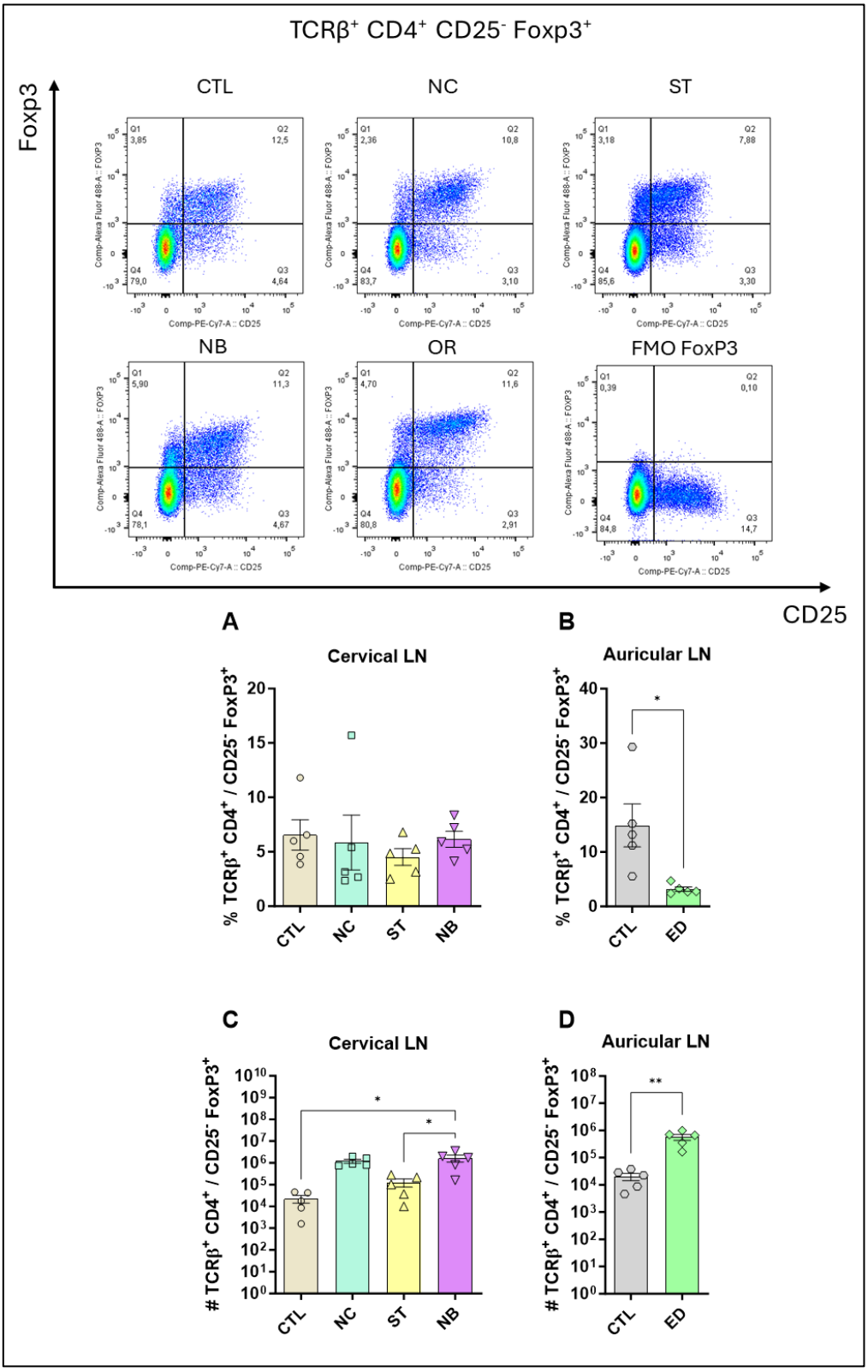

633 **Figure S12. TCRβ^{+} CD4^{+} CD25^{-} FoxP3^{+} profile.** The figure shows the representatives and
634 graphs with the percentage of cells in the nasal and ear sites (A) and (B) respectively. In (C) and
635 (D) data on the total number of cells are represented. Data of one independent experiment.
636 Statistics: plot with Standard Error of The Mean (SEM), t-test was used for all groups and samples
637 * p<0,05, **<0,005., 3-6 animals per group in each.

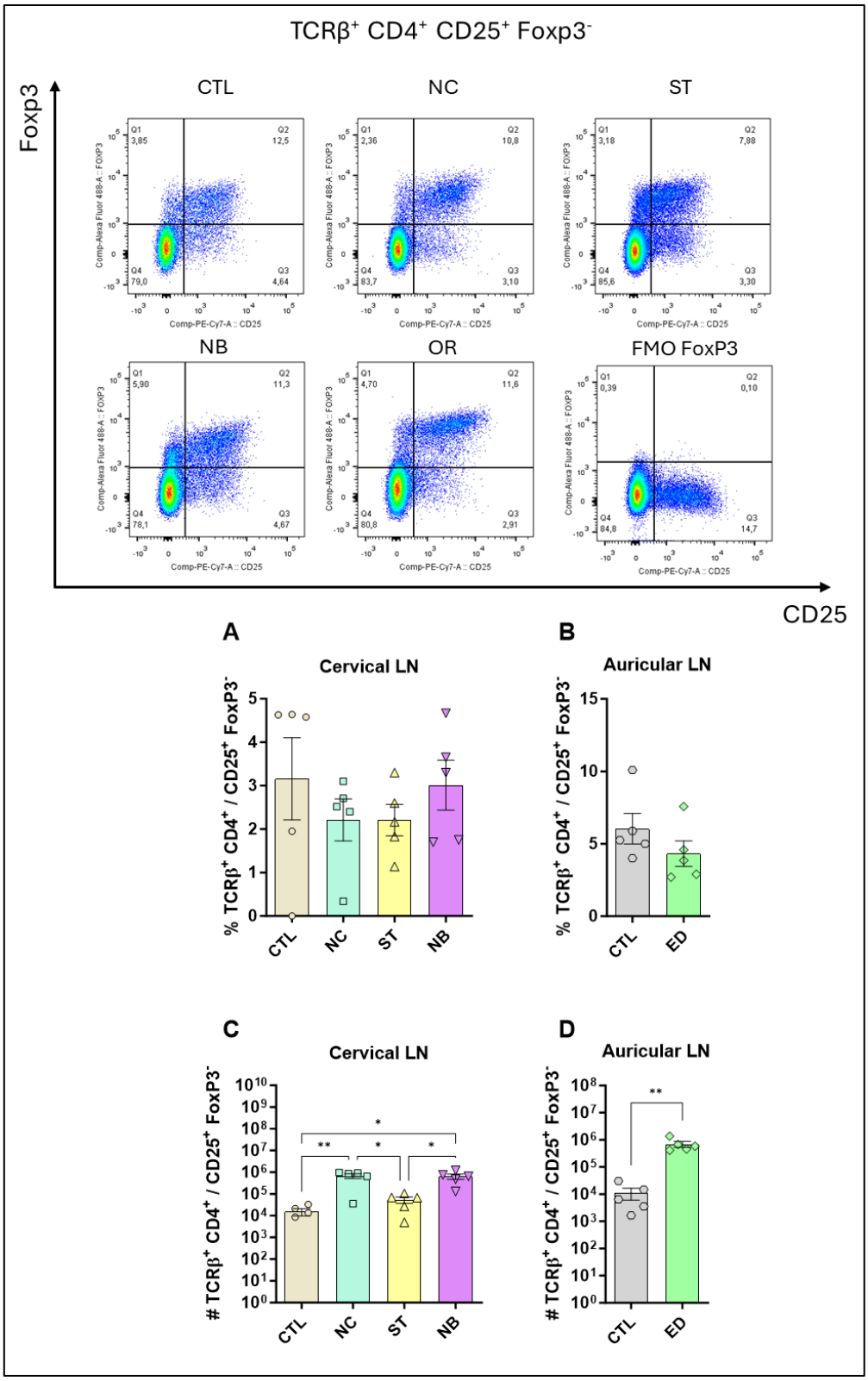

Figure S13. TCRβ⁺ CD4⁺ CD25⁺ FoxP3⁻ profile. The figure shows the representatives and graphs with the percentage of cells in the nasal and ear sites (A) and (B) respectively. In (C) and (D) data on the total number of cells are represented. Data of one independent experiment.

642 Statistics: plot with Standard Error of The Mean (SEM), t-test was used for all groups and samples

643 * p<0,05, **<0,005., 3-6 animals per group in each.

644

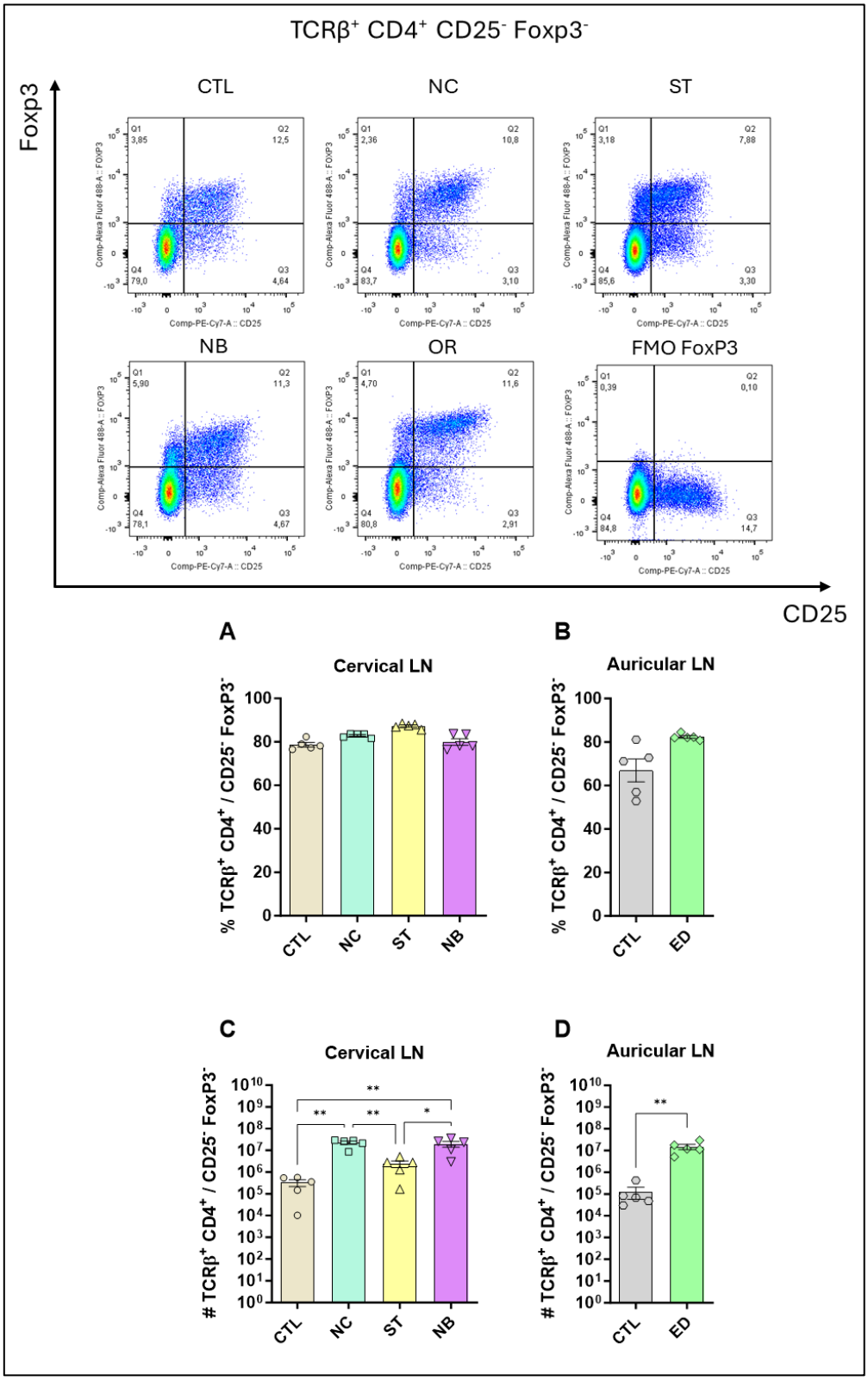

645

646 **Figure S14. TCRβ^{+} CD4^{+} CD25^{-} FoxP3^{-} profile.** The figure shows the representatives and
647 graphs with the percentage of cells in the nasal and ear sites (A) and (B) respectively. In (C) and
648 (D) data on the total number of cells are represented. Data of one independent experiment.
649 Statistics: plot with Standard Error of The Mean (SEM), t-test was used for all groups and samples
650 * p<0,05, **<0,005., 3-6 animals per group in each.

651

652

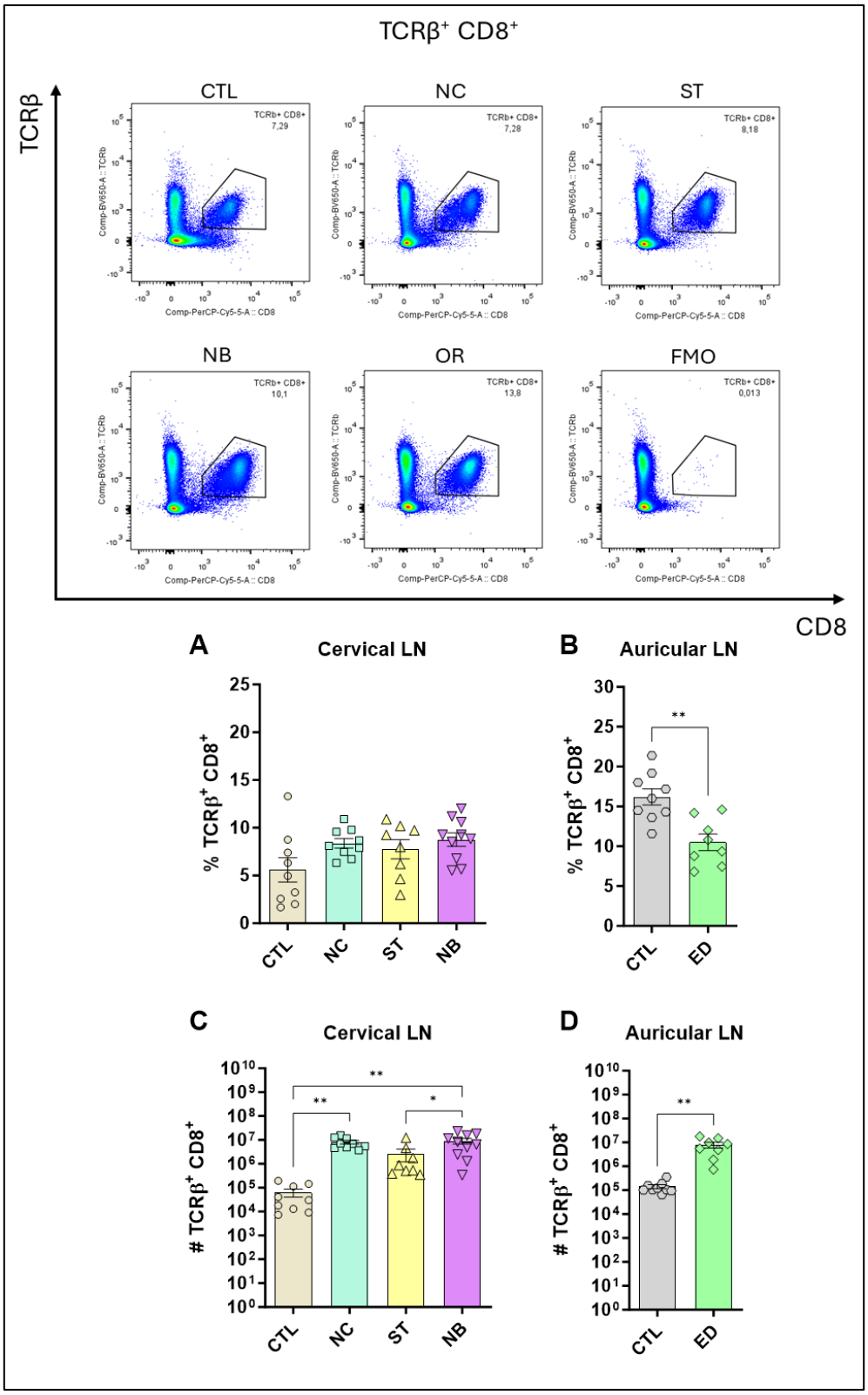

Figure S15. Profile of TCRβ⁺ CD8⁺ Cells. The figure shows the representatives and graphs with the percentage of cells in the nasal and ear sites (A) and (B) respectively. In (C) and (D) data on the total number of cells are represented. Data accumulative of two independent experiments.

Statistics: plot with Standard Error of The Mean (SEM), t-test was used for all groups and samples * p<0,05, **<0,005., 3-6 animals per group in each.

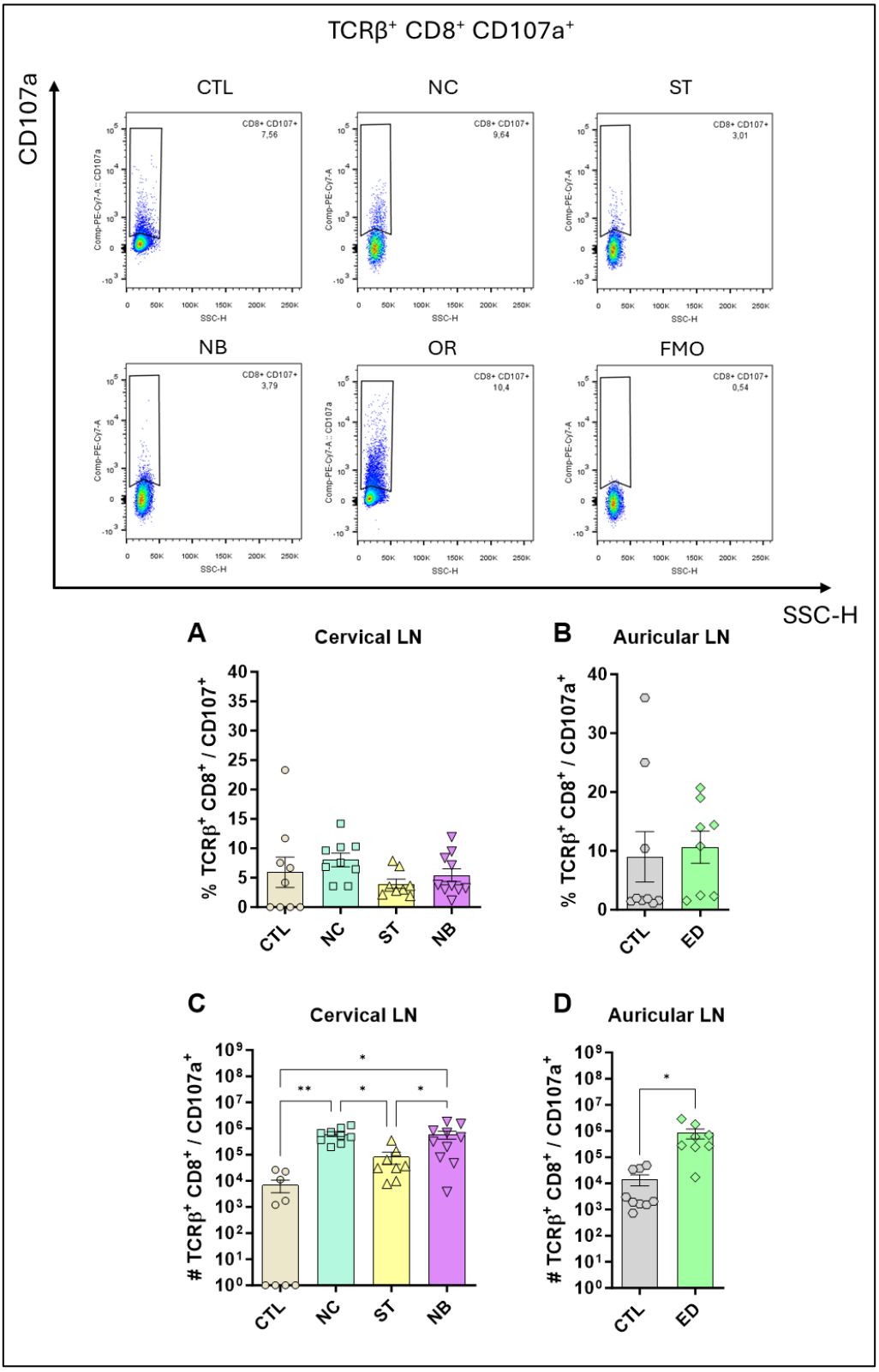

661 **Figure S16. Profile of TCRβ^{+} CD8^{+} CD107a^{+} Cells.** The figure shows the representatives and
662 graphs with the percentage of cells in the nasal and ear sites (A) and (B) respectively. In (C) and
663 (D) data on the total number of cells are represented. Data accumulative of two independent
664 experiments. Statistics: plot with Standard Error of The Mean (SEM), t-test was used for all groups
665 and samples * p<0,05, **<0,005., 3-6 animals per group in each.

666

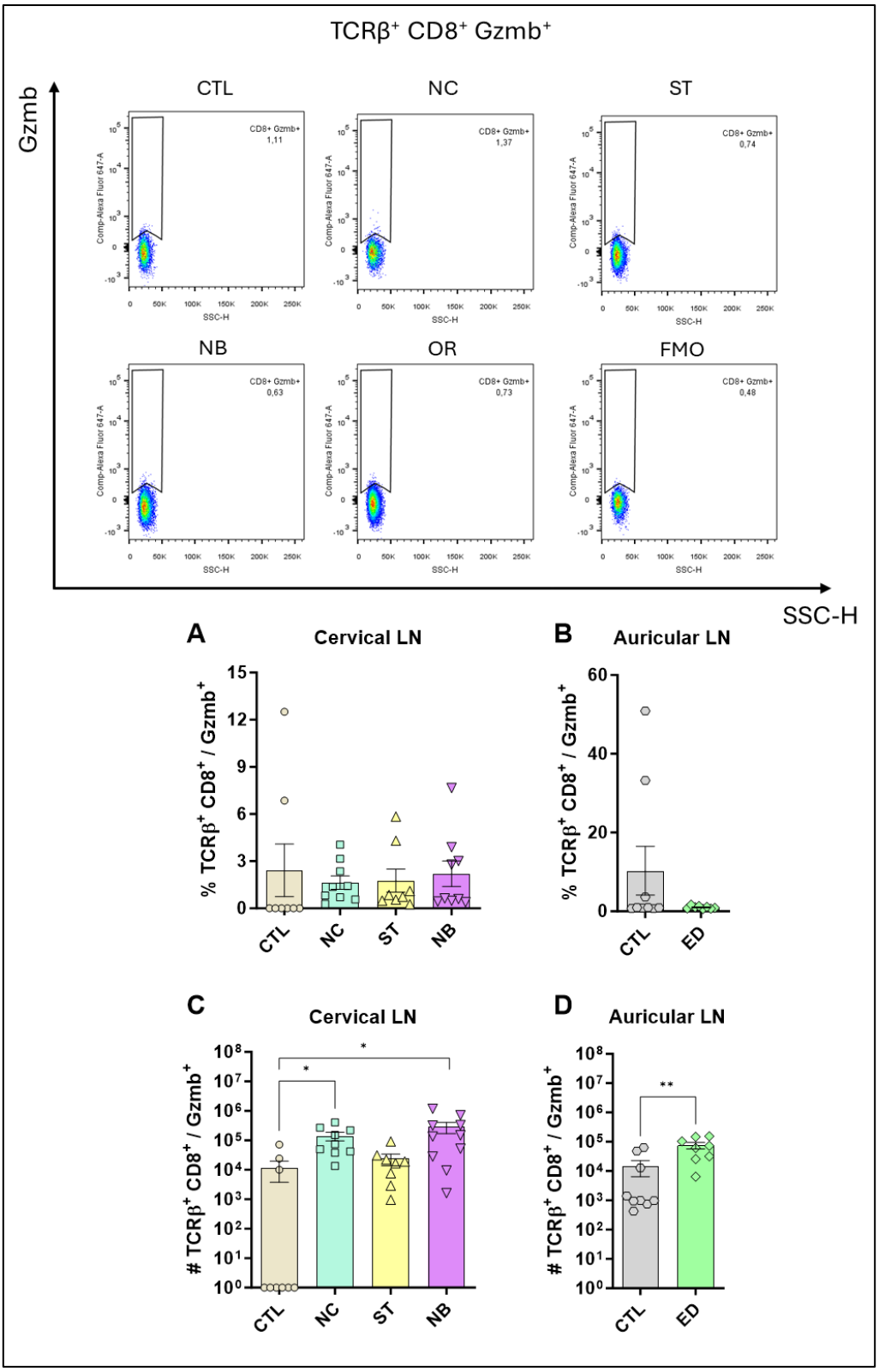

667

668 **Figure S17. Profile of TCRβ⁺ CD8⁺ Gzmb⁺ Cells.** The figure shows the representatives and
669 graphs with the percentage of cells in the nasal and ear sites (A) and (B) respectively. In (C) and
670 (D) data on the total number of cells are represented. Data accumulative of two independent

experiments. Statistics: plot with Standard Error of The Mean (SEM), t-test was used for all groups and samples * p<0,05, **<0,005., 3-6 animals per group in each.

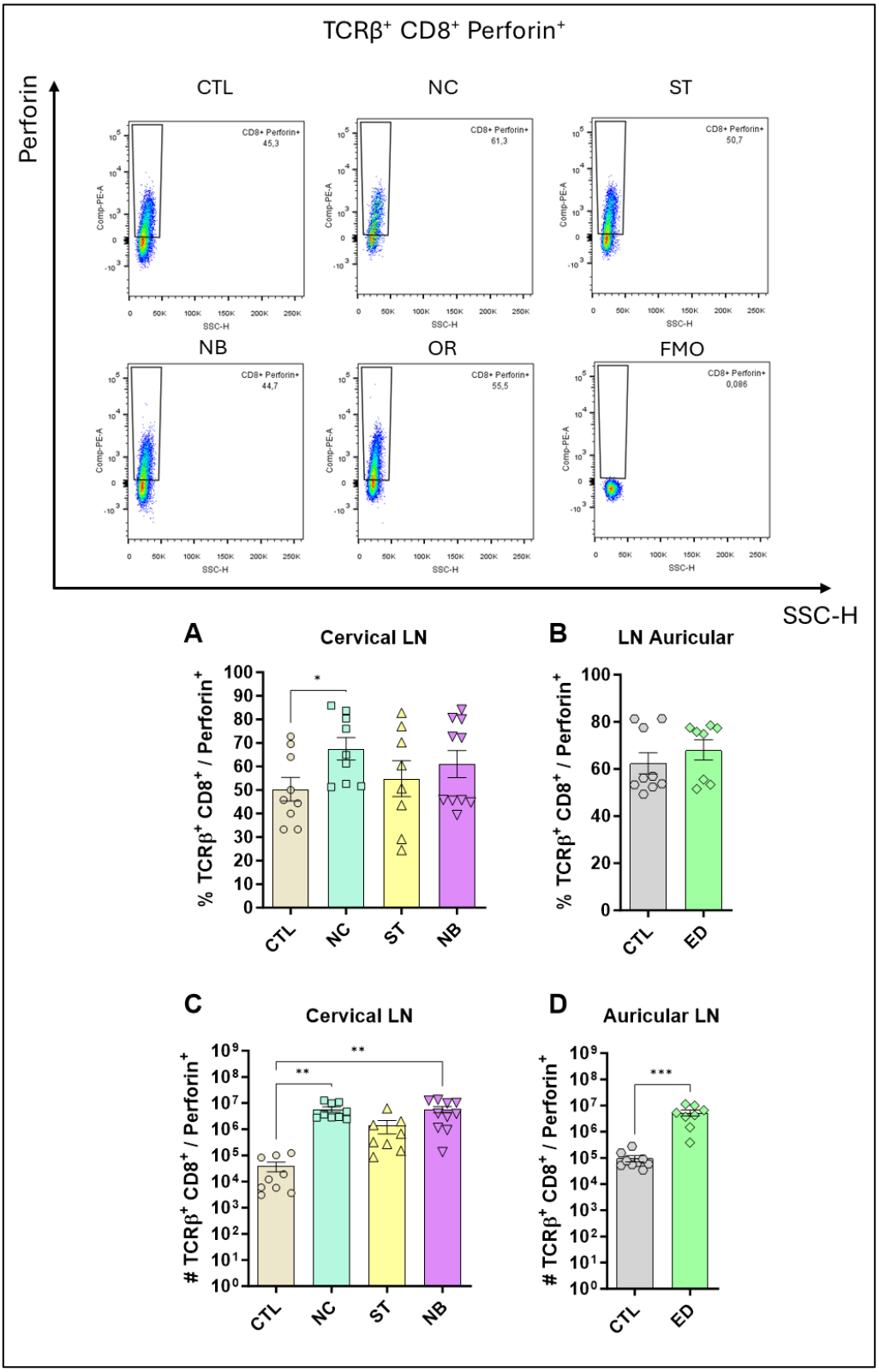

675 **Figure S18. Profile of TCRβ^{+} CD8^{+} Perforin^{+} Cells.** The figure shows the representatives and
676 graphs with the percentage of cells in the nasal and ear sites (A) and (B) respectively. In (C) and
677 (D) data on the total number of cells are represented. Data accumulative of two independent
678 experiments. Statistics: plot with Standard Error of The Mean (SEM), t-test was used for all groups
679 and samples * p<0,05, **<0,005., 3-6 animals per group in each.

680

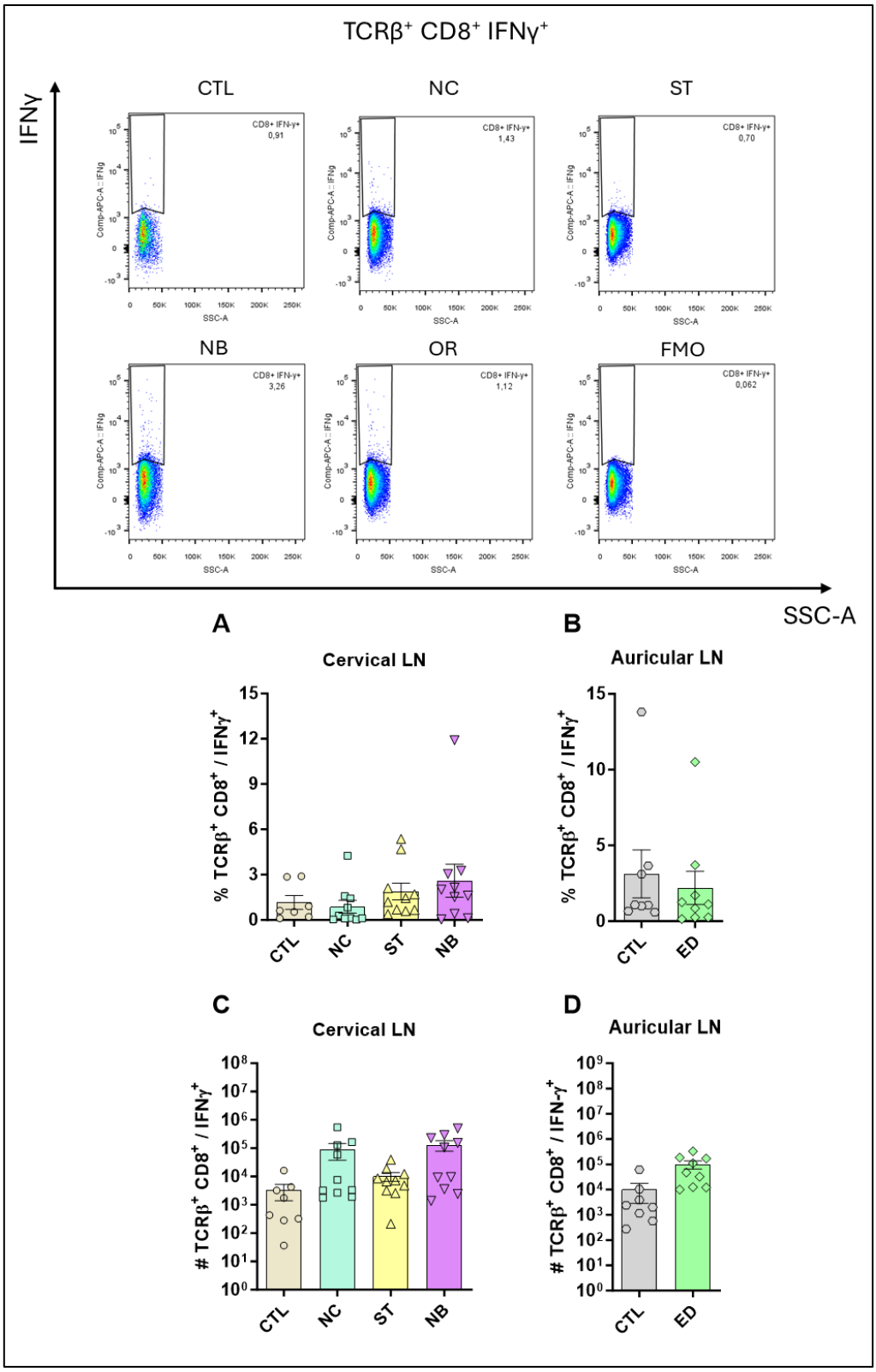

681

682 **Figure S19. Profile of TCRβ⁺ CD8⁺ IFN-γ⁺ Cells.** The figure shows the representatives and
683 graphs with the percentage of cells in the nasal and ear sites (A) and (B) respectively. In (C) and
684 (D) data on the total number of cells are represented. Data accumulative of two independent

experiments. Statistics: plot with Standard Error of The Mean (SEM), t-test was used for all groups and samples * p<0,05, **<0,005., 3-6 animals per group in each.

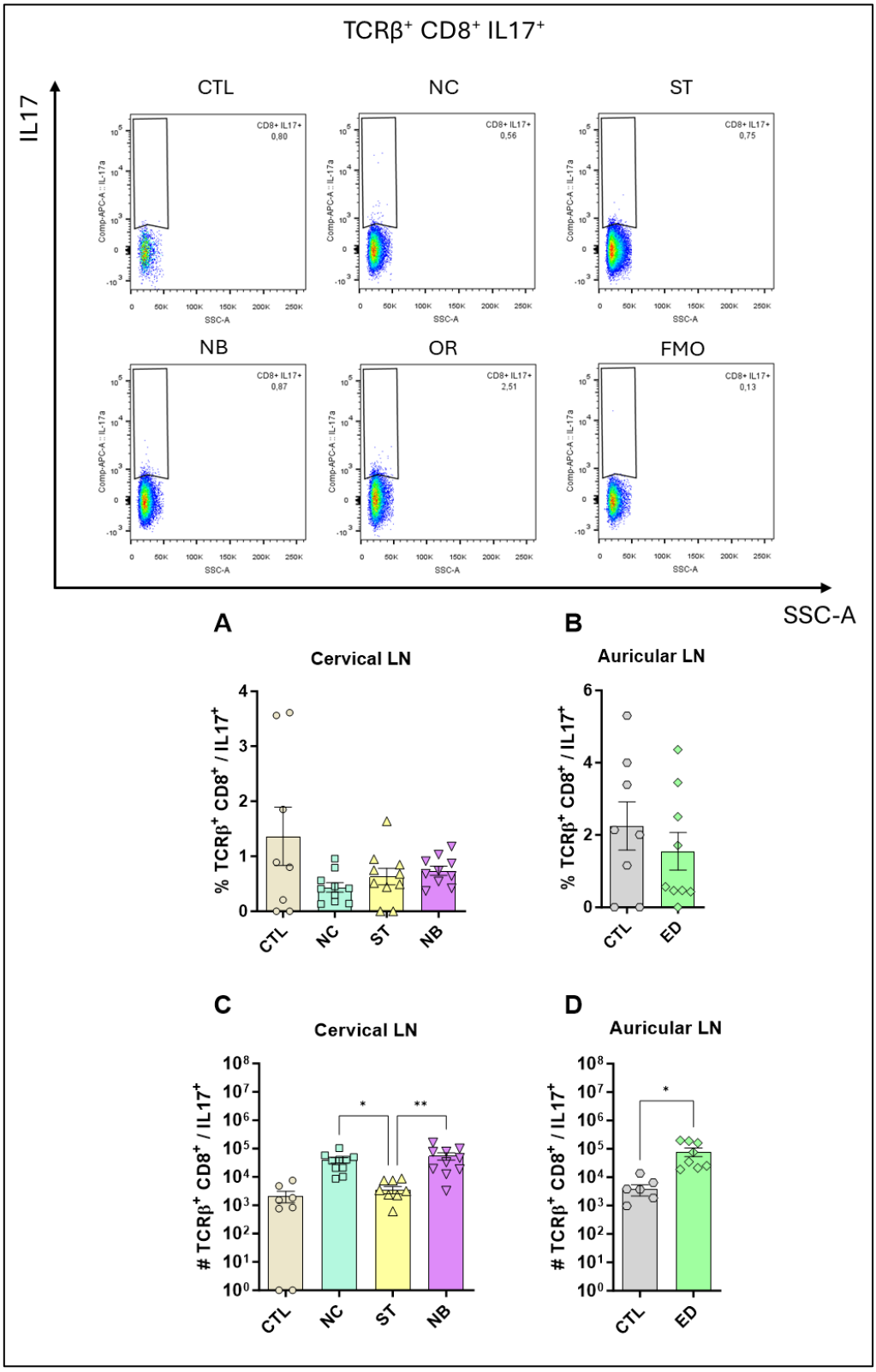

689 **Figure S20. Profile of TCRβ^{+} CD8^{+} IL-17^{+} Cells.** The figure shows the representatives and
690 graphs with the percentage of cells in the nasal and ear sites (A) and (B) respectively. In (C) and
691 (D) data on the total number of cells are represented. Data accumulative of two independent
692 experiments. Statistics: plot with Standard Error of The Mean (SEM), t-test was used for all groups
693 and samples * p<0,05, **<0,005., 3-6 animals per group in each.

694

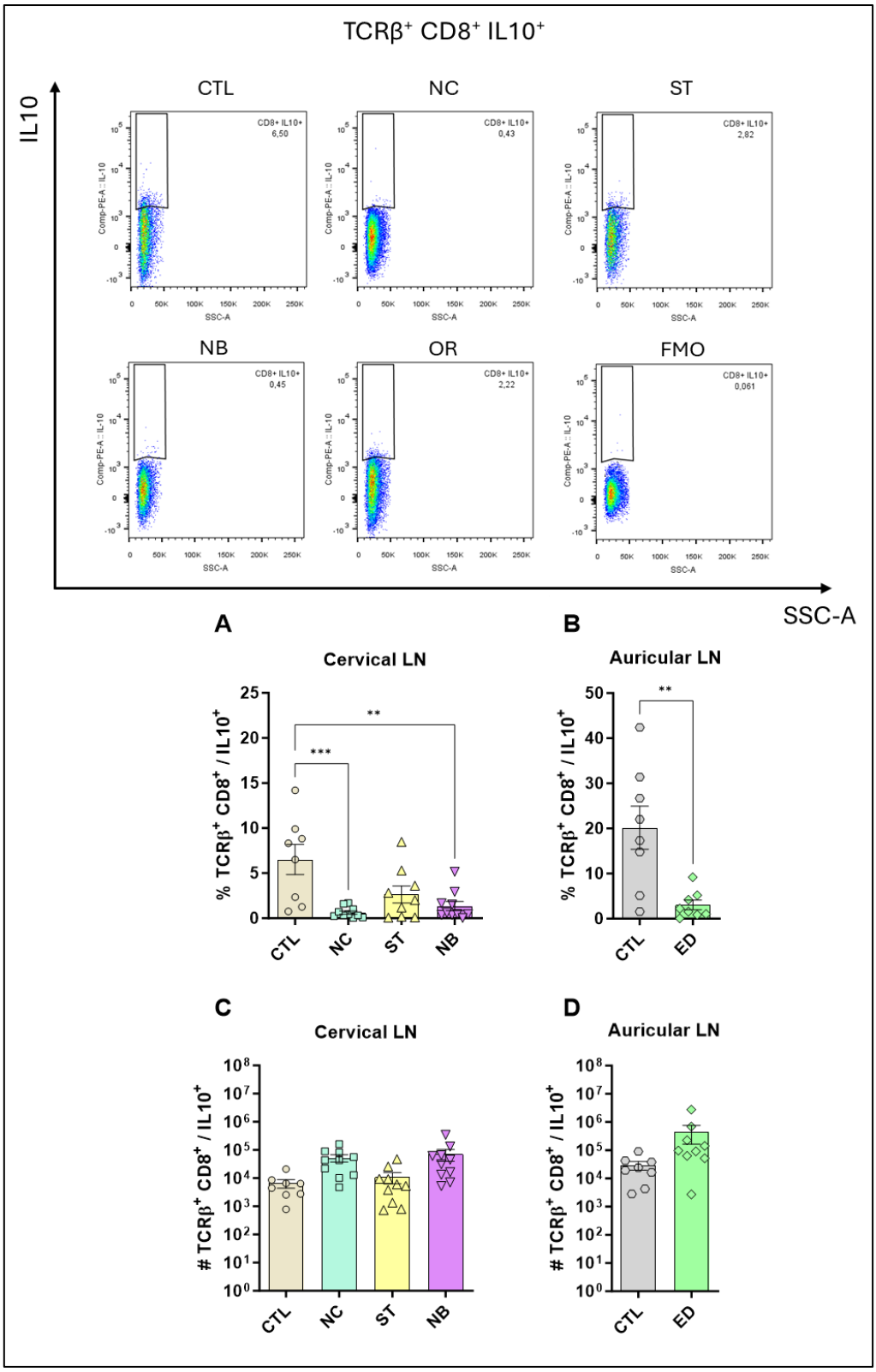

695

696 **Figure S21. Profile of TCRβ⁺ CD8⁺ IL-10⁺ Cells.** The figure shows the representatives and
697 graphs with the percentage of cells in the nasal and ear sites (A) and (B) respectively. In (C) and
698 (D) data on the total number of cells are represented. Data accumulative of two independent

experiments. Statistics: plot with Standard Error of The Mean (SEM), t-test was used for all groups and samples * p<0,05, **<0,005., 3-6 animals per group in each.

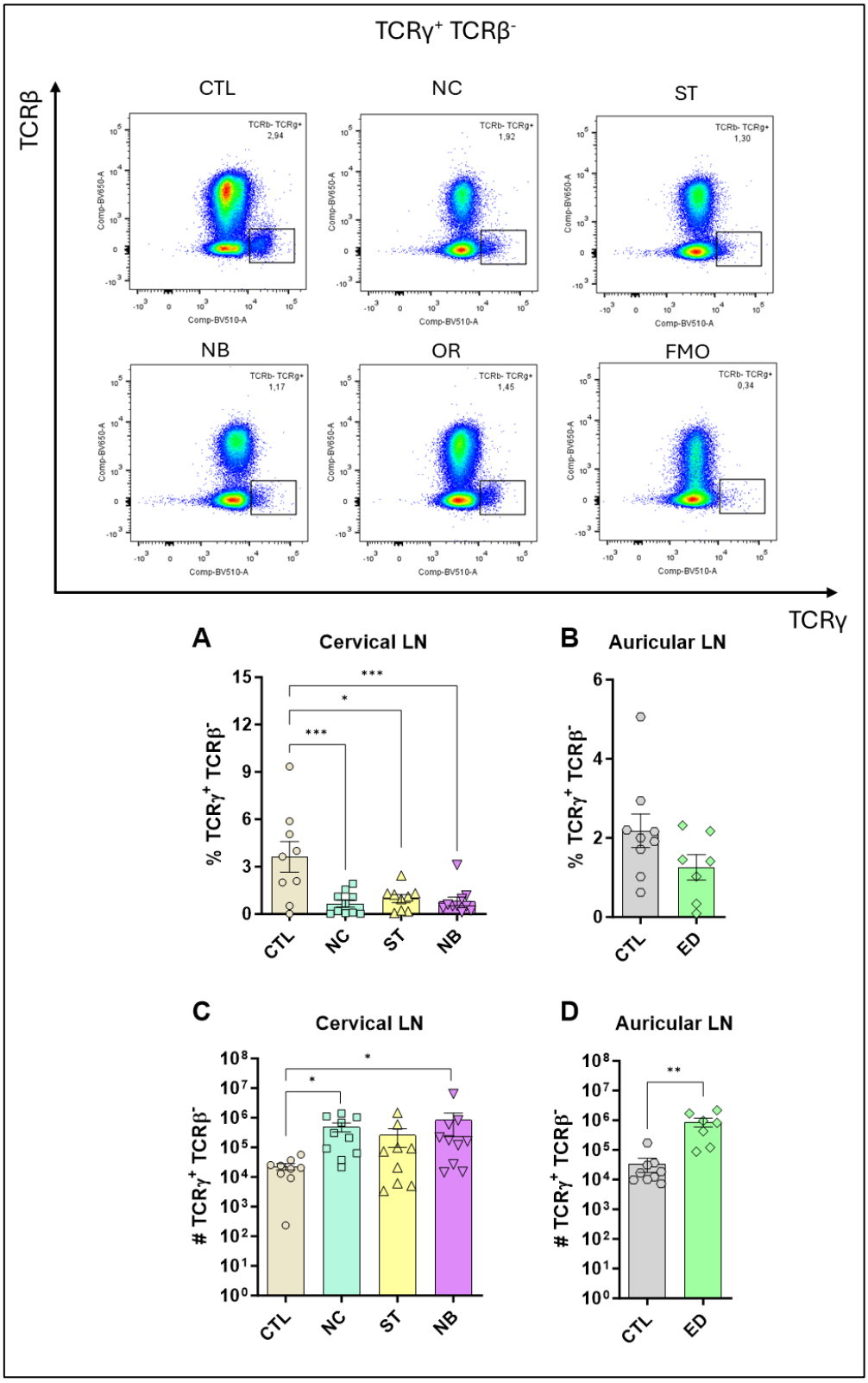

Figure S22. Profile of TCRγ^{+} TCRβ^{-} Cells. The figure shows the representatives and graphs with the percentage of cells in the nasal and ear sites (A) and (B) respectively. In (C) and (D) data on the total number of cells are represented. Data accumulative of two independent experiments. Statistics: plot with Standard Error of The Mean (SEM), t-test was used for all groups and samples * p<0,05, **<0,005., 3-6 animals per group in each.

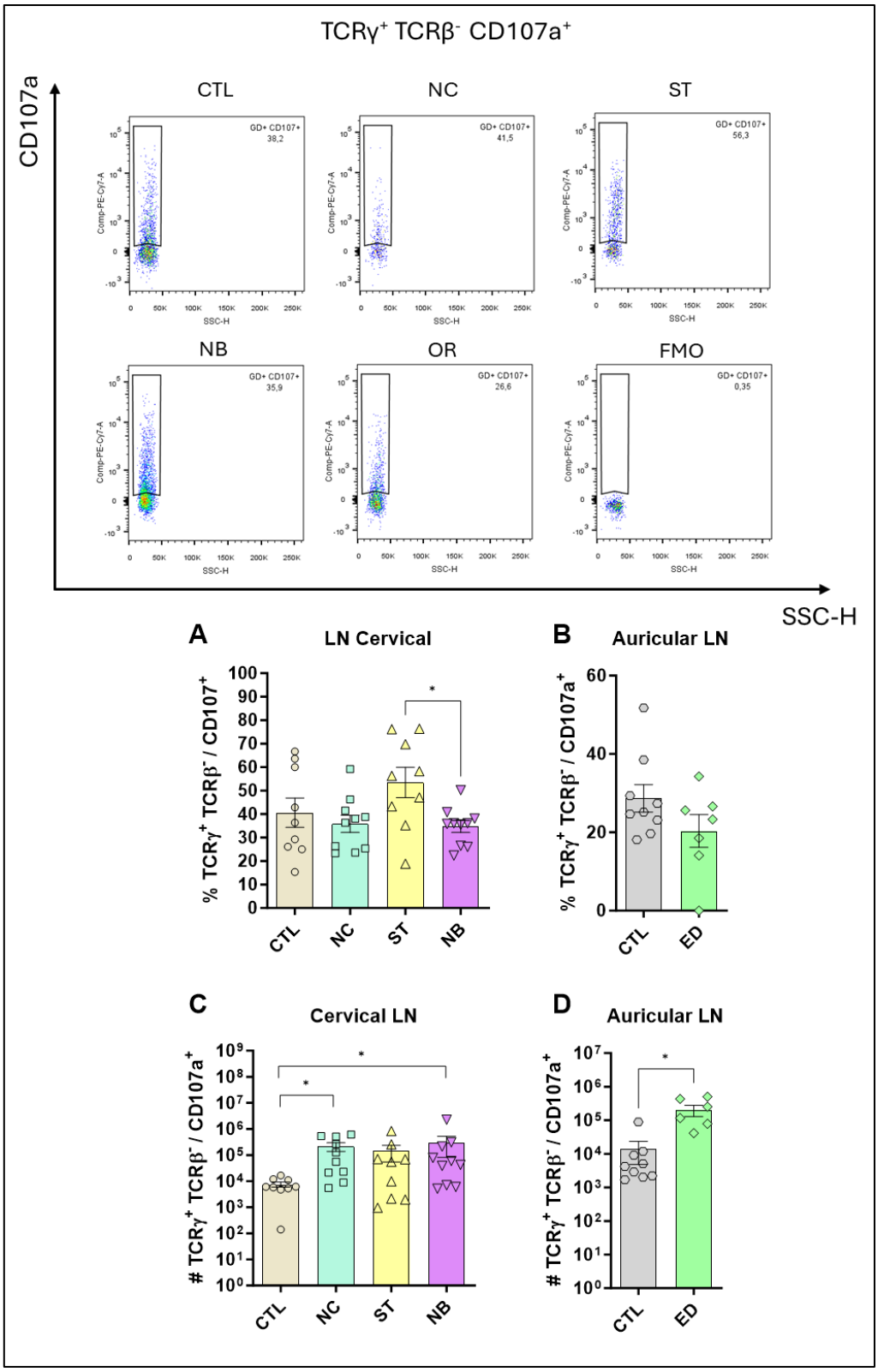

Figure S23. TCRγ⁺ TCRβ⁻ CD107a⁺ profile. The figure shows the representatives and graphs with the percentage of cells in the nasal and ear sites (A) and (B) respectively. In (C) and (D) data on the total number of cells are represented. Data accumulative of two independent experiments.

713 Statistics: plot with Standard Error of The Mean (SEM), t-test was used for all groups and samples

714 * p<0,05, **<0,005., 3-6 animals per group in each.

715

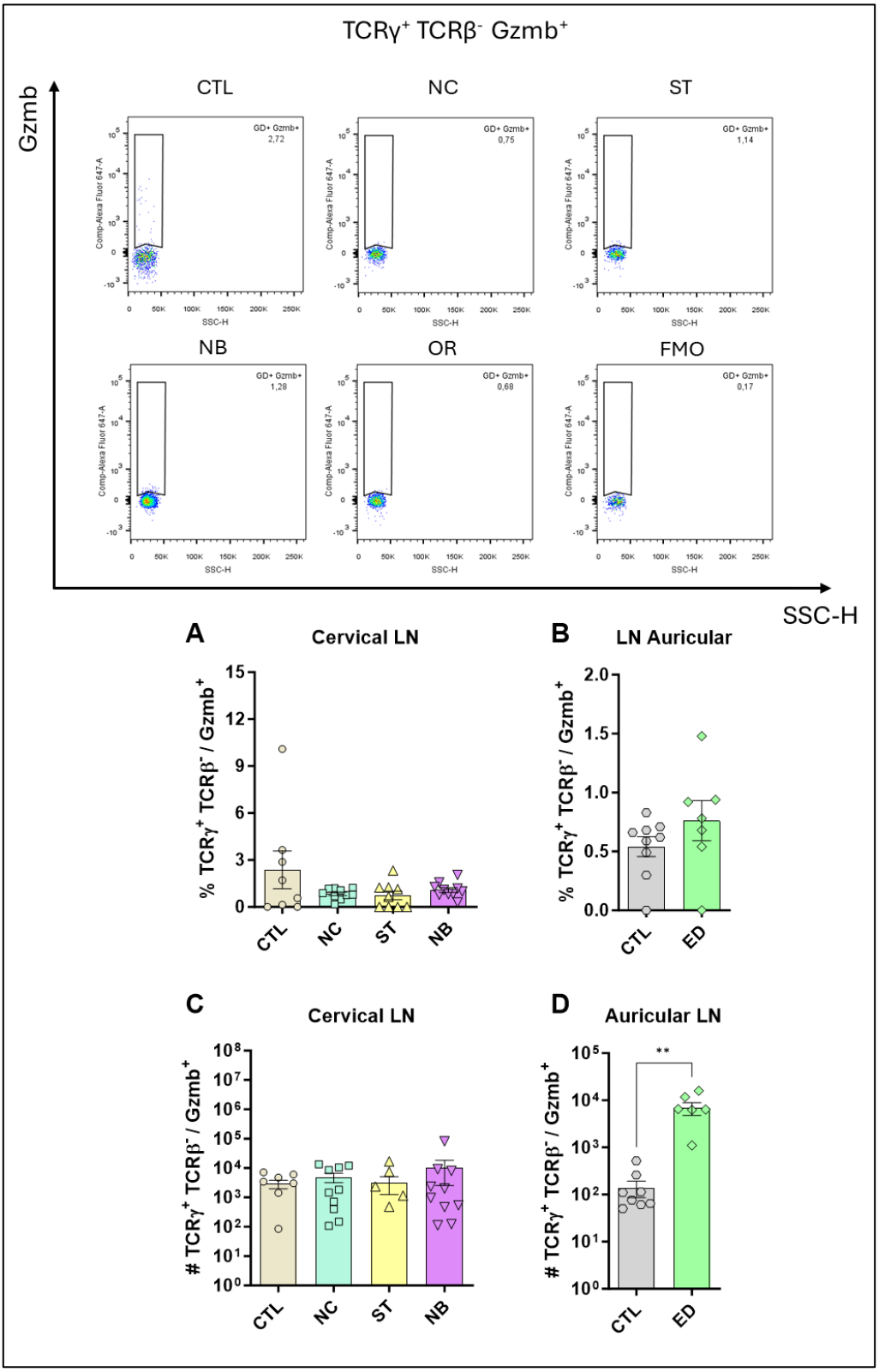

716

717 **Figure S24. TCRγ^{+} TCRβ^{-} Gzmb^{+} profile.** The figure shows the representatives and graphs with
718 the percentage of cells in the nasal and ear sites (A) and (B) respectively. In (C) and (D) data on
719 the total number of cells are represented. Data accumulative of two independent experiments.
720 Statistics: plot with Standard Error of The Mean (SEM), t-test was used for all groups and samples
721 * p<0,05, **<0,005., 3-6 animals per group in each.

722

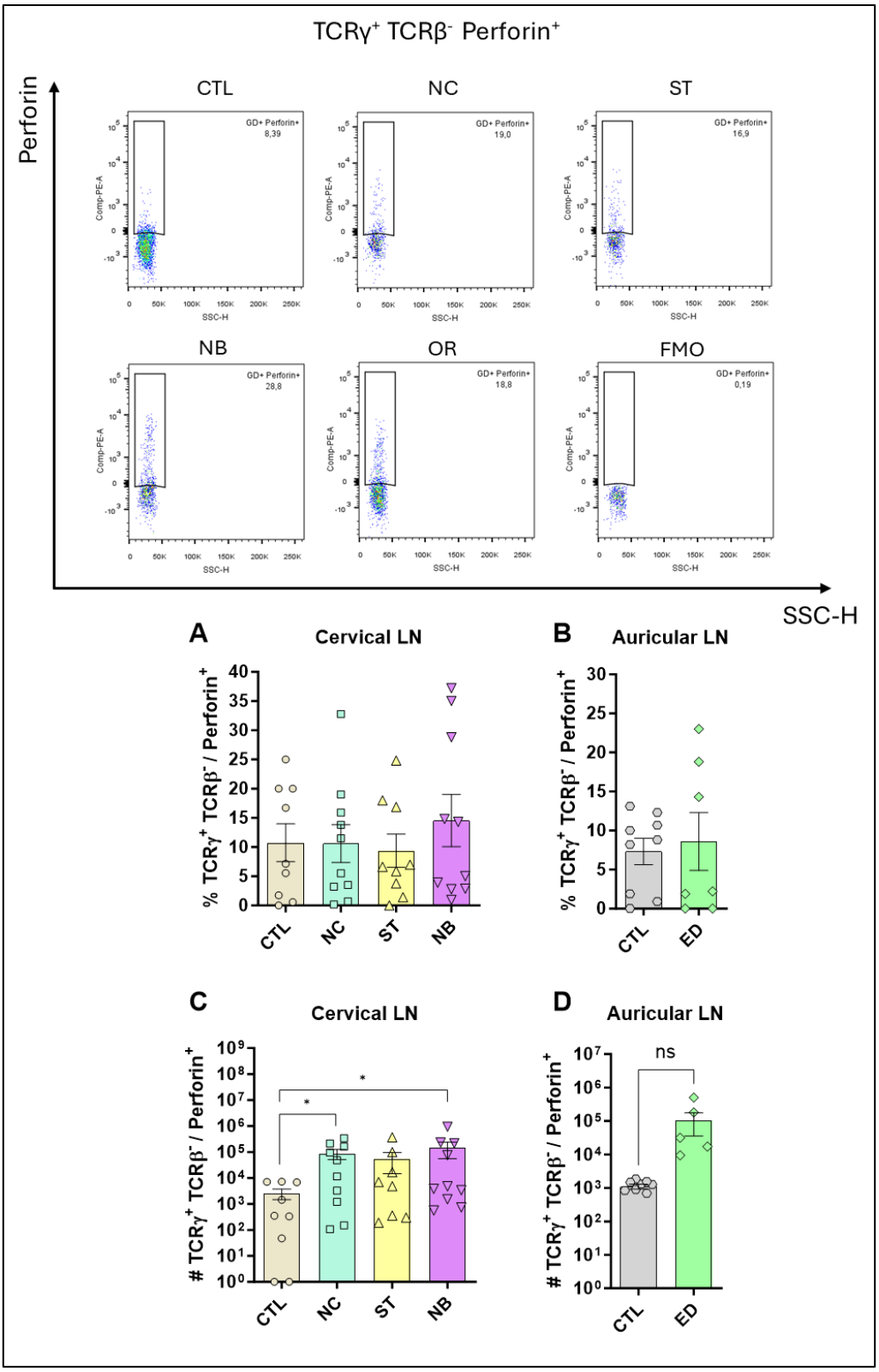

723

724 **Figure S25. TCRγ+ TCRβ- Perforin+ profile.** The figure shows the representatives and graphs
725 with the percentage of cells in the nasal and ear sites (A) and (B) respectively. In (C) and (D) data
726 on the total number of cells are represented. Data accumulative of two independent experiments.

Statistics: plot with Standard Error of The Mean (SEM), t-test was used for all groups and samples * p<0,05, **<0,005., 3-6 animals per group in each.

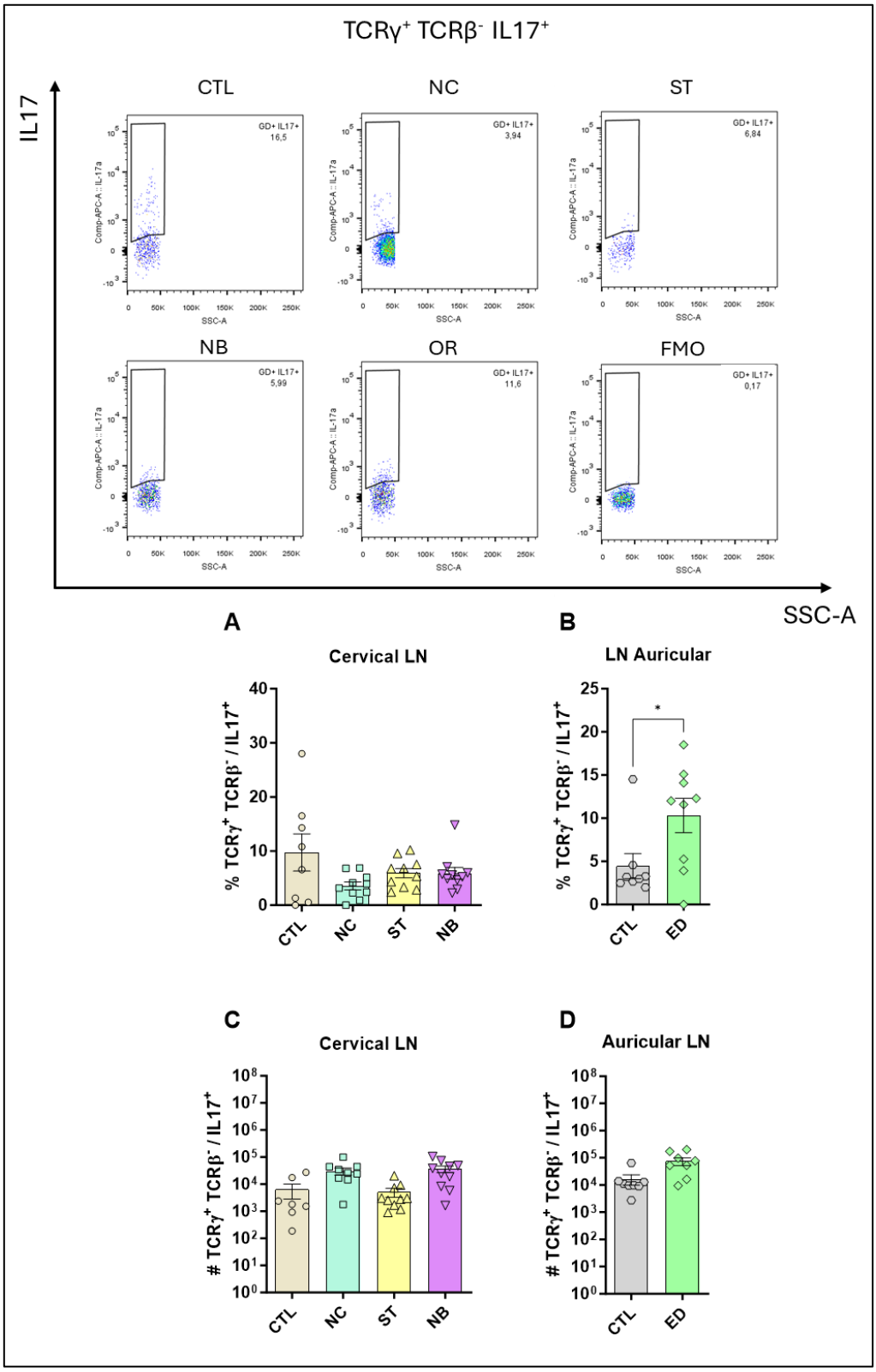

731 **Figure S26. TCRγ^{+} TCRβ^{-} IL-17^{+} profile.** The figure shows the representatives and graphs with
732 the percentage of cells in the nasal and ear sites (A) and (B) respectively. In (C) and (D) data on
733 the total number of cells are represented. Data accumulative of two independent experiments.
734 Statistics: plot with Standard Error of The Mean (SEM), t-test was used for all groups and samples
735 * p<0,05, **<0,005., 3-6 animals per group in each.

736

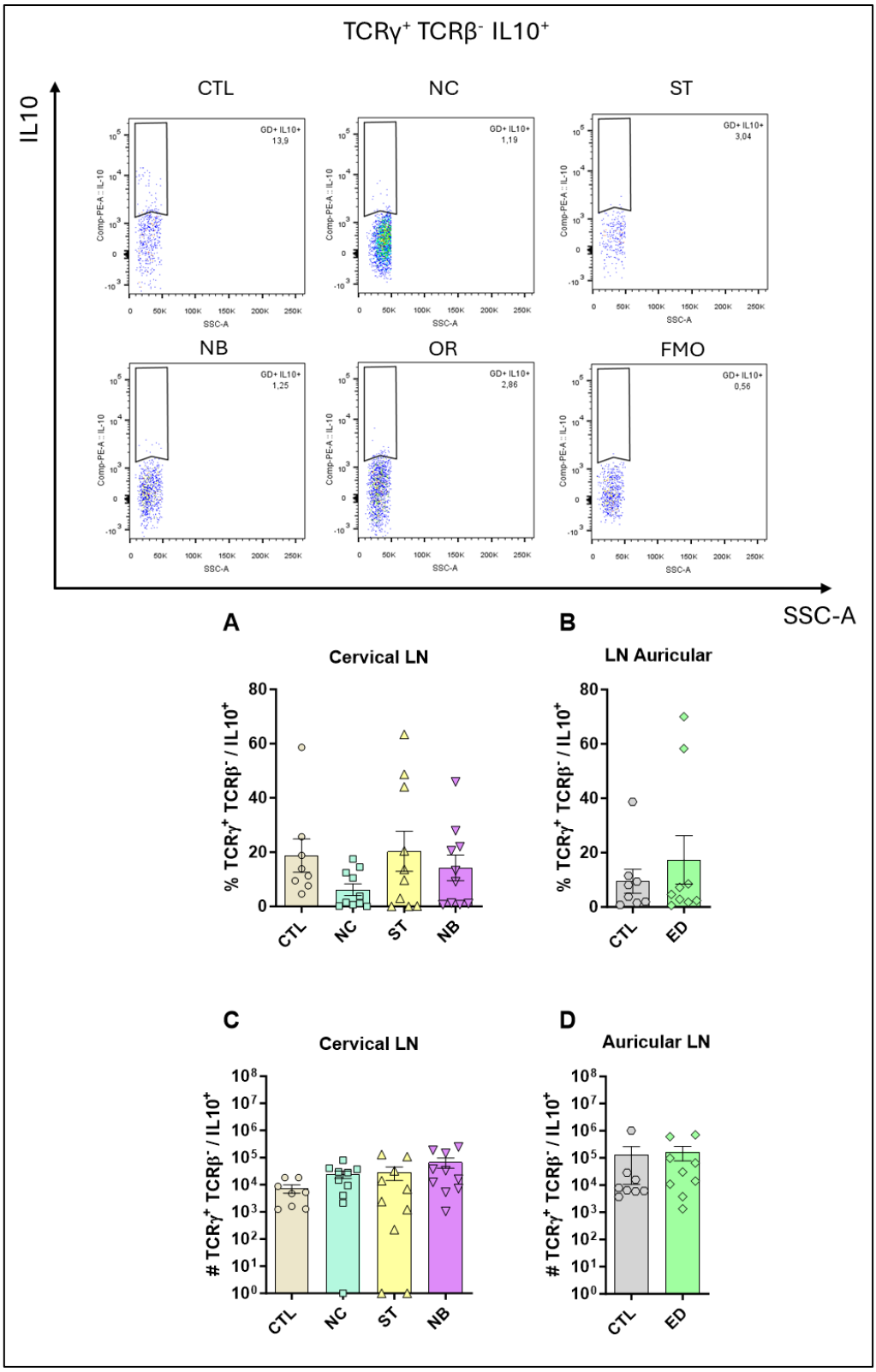

737

738 **Figure S27. TCRγ⁺ TCRβ⁻ IL-10⁺ profile.** The figure shows the representatives and graphs with

739 the percentage of cells in the nasal and ear sites (A) and (B) respectively. In (C) and (D) data on

740 the total number of cells are represented. Data accumulative of two independent experiments.

Statistics: plot with Standard Error of The Mean (SEM), t-test was used for all groups and samples * p<0,05, **<0,005., 3-6 animals per group in each.

Table S1. BD LSR Fortessa X20 Cytometer Lasers and Filters Configuration.

Laser	Filter BP	Filter LP	Laser	Filter BP	Filter LP
Violet	780/60 710/50 670/30 610/20 525/50 450/50	750 690 655 595 505 ---	**Yellow-Green**	780/60 710/50 670/30 60/20 586/15	750 685 635 600 ---
Blue	710/50 530/30	690 505	**Red**	780/60 730/45 670/30	750 710 ---

Table S2. Main staining antibodies markers, colors and concentrations.

Extracellular			Intracellular		
Antibody	**Fluorocrome**	**Concentration**	**Antibody**	**Fluorocrome**	**Concentration**
anti-CD3	BV605	1μg/mL	anti-IL-10	PE	2μg/mL
anti-CD4	BV785	1μg/mL	anti-IL-17	APC	2μg/mL
anti-CD8	Percp Cy5.5	1μg/mL	anti-IFN-γ	FITC	2μg/mL
anti-TCRβ	BV650	1μg/mL	anti-Perforin	PE	2μg/mL
anti-TCRγ	BV510	1μg/mL	anti-Granzyme b	APC	2μg/mL
anti-CD25	PE Cy7	1μg/mL	anti-CD107a	APC Cy7	2μg/mL
anti-PD-1	PE-Cy7	1μg/mL	anti-FoxP3	AF488	2μg/mL

747